

Article

Design and Analysis of a Variable Buoyancy System for Efficient Hovering Control of Underwater Vehicles with State Feedback Controller

Brij Kishor Tiwari  and Rajiv Sharma * 

Design and Simulation Laboratory, Department of Ocean Engineering, Indian Institute of Technology Madras, Chennai (TN) 600036, India; aeromantiwari@gmail.com

* Correspondence: rajivatri@iitm.ac.in

Received: 22 February 2020; Accepted: 4 April 2020; Published: 8 April 2020



Abstract: The design process for Variable Buoyancy System (VBS) is not known in full, and existing approaches are not scalable. Furthermore, almost all the small size Autonomous Underwater Vehicles/Gliders (AUVs/G's) use very low capacity of buoyancy change (in the range of few milliliters) and the large size AUVs require large buoyancy change. Especially for adverse weather conditions, emergency recovery or defense-related applications, higher rate of rising/sinking (heave velocity) is needed along with an ability to hover at certain depth of operation. Depth of UVs can be controlled either by changing the displaced volume or by changing the overall weight and, herein, our focus is on the later. This article presents the problem of design and analysis of VBS for efficient hovering control of underwater vehicles at desired depth using the state feedback controller. We formulate and analyze the design and analysis approach of VBS using the fundamental of mechanics, system dynamics integration and control theory. Buoyancy is controlled by changing the overall weight of the vehicle using the ballasting/de-ballasting of water in ballast tanks through the use of Positive Displacement Pump (PDP) for control in heave velocity and hovering depth. Furthermore, detailed mass metric analysis of scalable design of VBS for different buoyancy capacities is performed to analyze the overall performance of the VBS. Also, the performances of AUVs integrated with VBS of different buoyancy capacities are investigated in both the open loop and closed loop with the LQR state feedback controller. Hovering performance results are presented for three Design Examples (DEs) of AUVs with 2.8 m, 4.0 m and 5.0 m length and they are integrated with various buoyancy capacities at 9 kg/min rate of change of buoyancy. Results indicate that the AUVs achieve the desired depth with almost negligible steady state error and when they reach the desired hovering depth of 400 m the maximum pitch angle achieved of 16.5 degree for all the Des is observed. Maximum heave velocity achieved during sinking is 0.44 m/s and it reduces to zero when the vehicle reaches the desired depth of hovering. The presented computer simulation results indicate good performance and demonstrate that the designed VBS is effective and efficient in changing the buoyancy, controlling and maintaining the depth, controlling the heave velocity and can be used in rescue/attack operations of both the civil and defense UVs.

Keywords: variable buoyancy system (VBS); autonomous underwater vehicle (AUV); positive displacement pump (PDP); brush-less direct current (BLDC) motor; linear quadratic controller (LQR)

1. Introduction

A large area of the planet earth is occupied by oceans and they cover approximately 71% of Earth's surface and 90% of the Earth's biosphere. They contain 97% of Earth's water. Even though their importance is undeniable, they largely remain unexplored, i.e., less than 20% of the World Ocean has been explored [1].

This scene demands vehicles that can be used for surveying the oceans for high endurance and operable at high depths. These requirements have motivated the researchers to design and develop new age Underwater Vehicles (UVs). UVs are designed to perform underwater survey missions such as detecting and mapping submerged wrecks, rocks and obstructions that can pose a hazard, primarily for efficient navigation to be used in the commercial and recreational vessels, for launching torpedoes and rescue operations.

1.1. Background and Motivation

Except the Remotely Operated Vehicles (ROVs) and other hybrid vehicles that have an umbilical cable connecting the vehicle and mother-ship, all other UVs either carry the source of power on-board or are designed with self-propulsion mode. This scenario demands that the power on-board is utilized efficiently so that the endurance in terms of either range or operational abilities is optimized. Major areas of power consumption in the UVs are: propulsion, sensing, hotel loads and depth control through buoyancy changes [2]. Operations like depth control, trim adjustment, deep diving and adjustments for the changes in sea water density and maneuvering requirements demand a change in the vehicle's designed buoyancy.

From the basic principles of physics it is known that a very accurately buoyancy change can be achieved with the application of thrust application. In theory, the thruster can be located in the radial direction and that allows the delivery of thrust in any direction (360 degrees), but in practice it has serious limitations because only a few directions will have a buoyancy component in the delivered thrust and other components in certain direction will even contribute to increase in the drag. This is shown in Figure 1. Furthermore, the application of thrust is power intensive and for a system design for which power comes at a premium because of expensive and space constrained battery resources, power cannot be drained for buoyancy adjustment without seriously affecting the range and endurance adversely. Hence, alternate mechanisms for buoyancy control need to be explored.

1.2. Research Contribution

Design process for Variable Buoyancy System (VBS) is neither known in full nor existing approaches are scalable. In the existing literature on Variable Buoyancy System (VBS) most of the papers have not reported reproducible details. Furthermore, all of them have presented the results as design summaries and the process at arriving on the design values has not been mentioned in any existing research. Nevertheless, with the available details, a brief list of limitations in the existing research is reported Table 1.

Table 1. List of the Underwater Vehicles (UVs) that use the Variable Buoyancy System (VBS) and their limitations.

S. No.	Applications	Description	Limitations	References
1	The first AUV developed for laying the fiber-optic cable on the sea bed.	$L = 10.7 \text{ m}$, $D = 1.27 \text{ m}$, Variable ballast tank capacity = 95 kg, Design depth = 1000 m.	- No design approach is reported. - The solution of very large capacity pump-driven VBS is restricted to only large size AUVs.	Ferguson [3] (Theseus AUV)
2	The AUV is employed for the environmental monitoring, marine science survey.	$L = 8.66 \text{ m}$, $D = 0.97 \text{ m}$, Design depth = 1000 m, Change in the net buoyancy capacity (B) = 90.72 kg	- No design approach is reported. - Designed application range is low depth and can be applied only for large size of the AUVs.	Tangirala and Dziedzki [4] (Seahorse AUV)
3	The AUV is employed for the oceanographic survey and seabed mapping.	$L = 10.6 \text{ m}$, $W = 2.55 \text{ m}$, $H = 2.4 \text{ m}$, Design depth = 3500 m, Buoyancy change capacity of up to 60 kg	- No design approach is reported. - Application is restricted to very deep water depths because of oil. - Integration with dynamics and CAD definition of the AUVs is not investigated.	Aoki et al. [5] (Urashima AUV)
4	The AUV is employed for the environmental monitoring, oceanographic survey.	$L = 2.29 \text{ m}$, $D = 0.305 \text{ m}$, Design depth = 300 m, Capable of trimming and drifting in a low power mode.	- No design approach is reported. - The application of VBS is only for the trimming of the AUV. - The design solution is restricted to very small changes in buoyancy.	Hobson et al. [6] (Tethys class long range AUV)

explored.

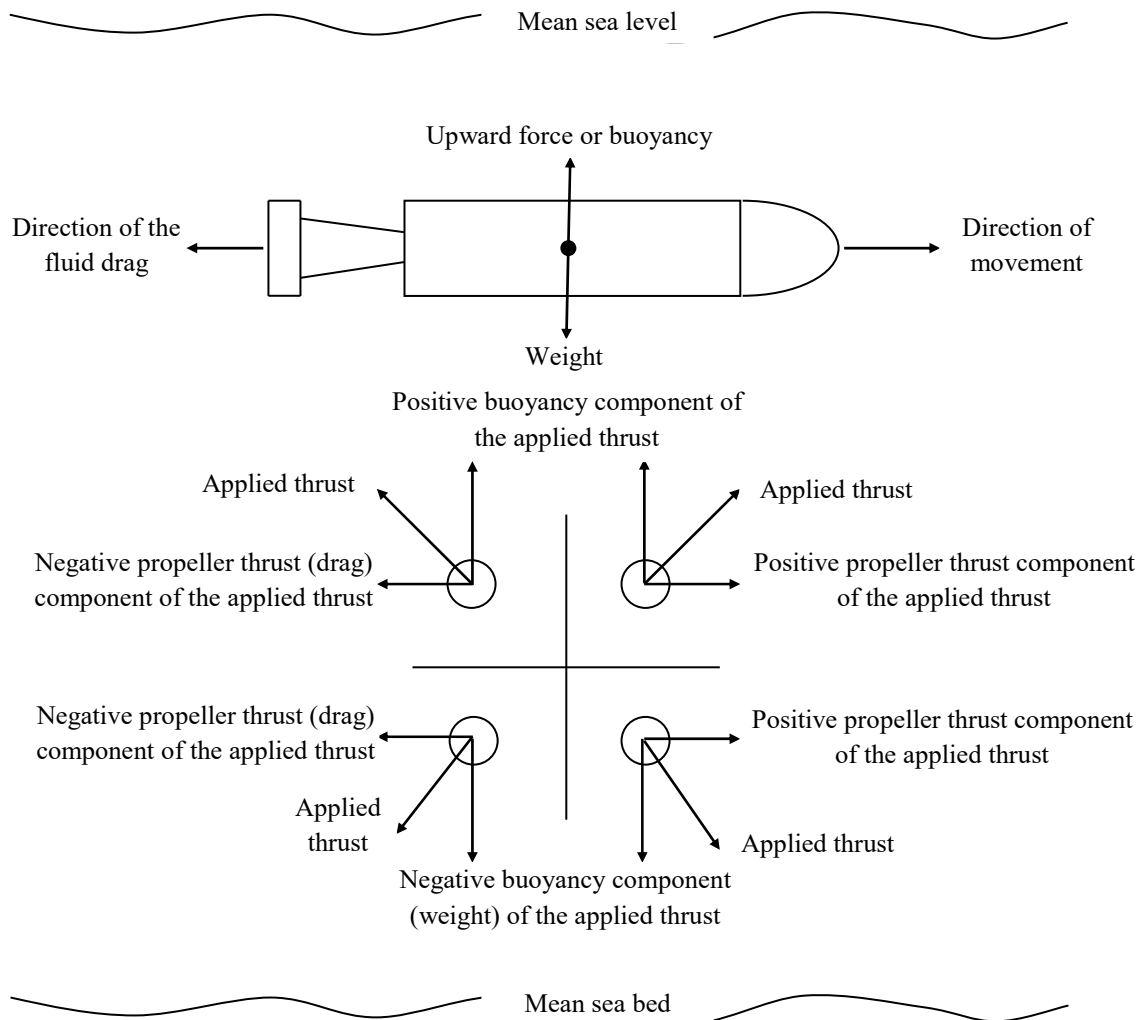


Figure 1. Schematic diagram to illustrate the buoyancy control with applied thrust.

Additionally, the concept of VBS looks deceptively simple to implement, but it has serious practical limitations while in either design or fabrication or both. For example, the MBARI vertical profiler uses a single hollow piston that reciprocates in order to directly change the volume of displacement related to the vehicle. This implies that they are starting with a screw/piston that is completely inside in the neutrally buoyant condition.

Later, while moving, it will move out of body and that will cause volumetric expansion. We note here that this design can be used only for the shallow water depths (i.e., less than 200 m) and for very low capacities of the required changes in buoyancy [7].

In Sumantr et al. [8] for the design of variable ballast mechanism for UVs a movable plate inside the ballast tank is used. This results in the change of volume of the ballast tank as the plate movement restricts/enhances the flow into the ballast tank. One side (bottom) is ensured to be always filled with the water and only the other side results in the variable change. We note here that this idea faces extreme challenges for the deep water depth applications in terms of energy efficiency and system reliability.

Some design concepts have relied upon the use of compressed air chambers and by the blowing/venting mechanism water volume can be displaced in many AUVs. Note that this design concept is only one way, i.e., once the compressed air is released the compressed air cannot be refilled

back in the underwater locations. Also, during the application stages due to the loss of pressure in the pressure chamber [9], it will become difficult to operate the system against high hydrostatic pressure. Furthermore, the design is complex, suits only large AUVs and it suffers from the usages of complicated mechanism resulting into low overall reliability.

Another type of the VBS as discussed by Woods et al. [10] used both the compressed air and water pump. Nevertheless, because of the coupling effect of hydraulics and pneumatics, a complex control mechanism was required and that results in high system complexity and low reliability.

Later for deep water depth operations in the ocean, a VBS was proposed by Worall et al. [11] for depth up to 6000 m and 30 kg buoyancy capability. In their work, no results were reported for the performance of AUV integrated with its VBS either through simulation or experimental testing. A Water Hydraulic Variable Buoyancy System (WHVBS) was proposed for very large capacity of buoyancy change using the swash plate radial piston pump by Liu et al. [12].

Nevertheless, this design idea is only limited to the VBS of very large capacity, applicable to only large AUVs and the authors did not report analysis for the performance of AUV integrated with its VBS either through simulation or experimental testing.

Based upon our critical examination of the existing literature, we note the following:

- No scalable design and analysis of the VBS has been proposed so far.
- There exists lack of clarity and application oriented understanding for the application of VBS to medium size of AUVs. Existing researches (in the form of design summaries only) exist either for very large capacity or very small capacity.
- Most of the WHVBS have the flow control through the on/off mode only, i.e., without controlling the flow rate of the water to/from the ballast tank. This process affects the performance and maneuverability of the AUVs in complex environment of the ocean, adversely.

In view of the limitations as mentioned above, our focus in this paper is to investigate the detailed design and development analysis of VBS which control the continuous mass flow rate. Mass metric analysis of the scalable design of VBS for different buoyancy capacity and computer simulation analysis of hovering performance of AUV integrated with designed VBS using efficient state feedback controller are studied in-detail. We conceive the computer simulation model in modules, each of the modules deals with a specific design process, modules are used to develop the mathematical design model and modules are integrated to achieve a seamless and integrated design simulation model. Our design application starts with the basic requirements and the dimensions of the AUVs/AUGs and ends with the detailed design of VBS suiting the specified requirements. Additionally, since our focus is on the requirements that are specific to the vehicle/glider (e.g., desired buoyancy changes are small for the AUG and large for the AUV, because of their differences in sizes), we present a model that is scalable, and the design approach is applicable for both. In our design application we study the buoyancy control in closed loop operation using the state feedback controller for efficient hovering control of AUV at a desired depth. An efficiency analysis for the overall design efficiency, applicability and uniqueness is reported in terms of the mass metric analysis of the VBS. Our idea is to improve the buoyancy capacity to weight ratio of the VBS, so that the payload weight of UVs can be improved. This is our contribution.

The remaining of this paper is organized: Section 2 discusses the modules in detail along with their mathematical models; Section 3 presents requirement and design features and detail metric analysis of the VBS; Section 4 presents integrated design and analysis of the AUV, VBS and controller; Section 5 presents simulation results and discussion; Section 6 presents verification and validation of the results and Section 7 describes the conclusions and future scope of research.

2. Basic Modular Structure of the Computer Simulation Model (CSM)

The basic modular structure of the CSM is shown in Figure 2. The CSM is conceived in four modules that are integrated seamlessly and output from one is input to the other. Module 1—Requirements of the VBS for UVs, methodology to control the buoyancy, design alternatives of the VBS as per

requirements; Module 2—mass metric analysis of the VBS, Mathematical modeling of the dynamics of AUV and its integration with the VBS; Module 3—Designed parameters of AUV and Controller design and Module 4—Conceptual design and simulation results—Open loop LQR controller and Closed loop LQR controller.

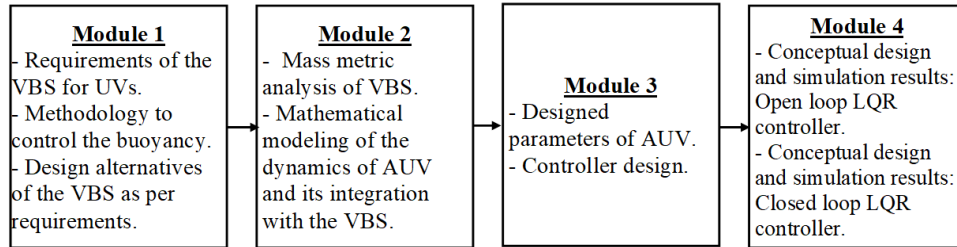


Figure 2. Basic modular structure of the Computer Simulation Model (CSM).

3. Requirement, Design Features and Detailed Metric Analysis of the VBS

3.1. Module 1.1—Requirements of the VBS for UVs

We note that the basic requirements of the VBS for UVs can be listed as the following:

- VBS is used for ensuring that the UV can be: Positively buoyant, negatively buoyant and accounts for the differences in buoyancy that will arise from the changes in the densities of fluids in which the UV is operating, e.g., river, lake, sea, ocean, and other water bodies all will have different densities.
- Change in the buoyancy without the use of thruster or any other mechanisms that will increase the drag, etc.
- Ensuring the hovering capability at any desired depth with zero forward speed, i.e., without operating the propellers
- Allowing the UV to achieve any desired heave velocity in different water bodies with high efficiency.
- Allowing, quick, efficient, and variable water depth operations for emergency release/recovery, especially for the defense applications.
- Ability to pitch control even at very low forward speed of the vehicle because at low speeds the control surfaces become inefficient.
- Integration of UV with VBS to ensure that it can reach up to/close to the bottom of the sea surface. This operation is efficiently neither possible with the usages of thruster or propeller, as all of them need sufficient clearances.
- Compensation for the weight of the AUVs which are used for laying the fiber optic cables during their operations or dropping off any other kind of the weight during the underwater operations (e.g., in this case large buoyancy capacity VBS is required to compensate for the weight).

3.2. Module 1.2—Methodology to Control the Buoyancy

Following Jensen [13] the buoyancy of a floating object is as follows:

$$\Delta B = (F_B - F_G) / g = M - \nabla \rho \quad (1)$$

where ΔB is the net buoyancy in kg, F_G is the gravitational force, F_B is the buoyant force because of the fluid on floating object, M is the total mass of the floating object, ∇ is the volume of the fluid displaced by the floating object, and ρ is the density of the fluid. The same is also valid for the submerged objects. A closer analysis of Equation (1) reveals that there are two approaches to control the buoyancy and they are:

- Change in the ∇ : In this approach, the idea is to control the buoyancy of vehicle by controlling the volume displaced by it. From the design perspective it implies that the shape of submerged/floating

object needs to change, i.e., either contraction or expansion. And, because of this the implementation of this idea will need flexible bladder, oil tank, Positive Displacement Pump (PDP), and Brush Less Direct Current (BLDC) motor, etc. We pump oil from the oil tank to the flexible bladder in order to increase the volume of fluid displaced by vehicle and thereby increasing the buoyancy and vice-versa Riedel et al. [14] and Webb et al. [15]. This concept has been used for some of the existing gliders, e.g., Sea glider—maximum volume change 840 cc, Slocum battery glider—maximum volume change 520 cc, and Spray glider—maximum volume change 900 cc Curtin et al. [16]; Wood and Stephen [17] and Davis et al. [18].

This idea appears simple but it has clear limitations, i.e., only a small amount of buoyancy can be changed. Also, geometrically the large expansions/contractions are not feasible and the attachment of expansion volume by using balloons etc. is expected to increase the drag significantly and design of structural configuration will be extremely difficult for deeply submerged vehicles operating at the larger water depths. Hence, this is normally applicable to the vehicles operating at low water depths and small capacity for the buoyancy change.

- Change in the M : In this approach, the idea is to control the total mass of the vehicle, which can be achieved by: either using the dead weights (e.g., AQUA EXPLORER-2 AUV used two dead weight releaser each of 2 kg, Kojima et al. [19]) or using the ballasting/de-ballasting of buoyancy tanks that are carried inside the AUV/AUGs hull.

It is easy to remove dead weight but the limitation is that once it is dropped it cannot be recovered back into the vehicle/glider. Because of this, it is applicable to only the one way change of buoyancy, e.g., increase of the buoyancy. A periodic change in the buoyancy is not practical with this idea.

In the process of ballasting, fluid is taken inside the tank and in the de-ballasting the fluid is taken out from the tank and discharged to the sea/ocean, etc. As the fluid always moves from high pressure to low pressure the creation of pressure difference is integral to this design concept and for this purpose either piston or rotary pump is used. The use of reciprocating piston pump is preferred for low changes in buoyancy and the pump is preferred for high changes in buoyancy. The advantages with uses of the piston and rotary pump are their scalability and applicability to both ways change of buoyancy, e.g., increase/decrease of the buoyancy.

Herein, we focus on the idea of change in M through the use of piston and pump. Depending upon the desired changes in the buoyancy of vehicle/glider, M is increased with ballasting and decreased with de-ballasting. Our complete approach for the design and selection of the VBS is shown in Figure 3.

3.3. Module 1.3—Design Alternatives of the VBS as per Requirements

The design features and requirements of the VBS for the AUV/AUG will affect the design and selection of applicable design options for VBS. We focus on: ‘Design Option 1 (DO1)’—Piston-driven and ‘Design Option 2 (DO2)’—Pump-driven.

In the DO1—Piston-driven VBS—the components are: cylindrical ballast tank, piston actuating inside the cylindrical tank, linear actuator, power source and BLDC motor, etc. The size of the cylindrical ballast tanks depends upon the $\pm B$ and the maximum size of the tank is restricted by 80 percent of D_{\max} . Also, it is important that a symmetric arrangement is maintained (i.e., enforcing the use of twin tanks, instead of one) and they are ballasted and de-ballasted uniformly. And the buoyancy is changed by the movement of piston that is driven by the electric linear actuator and this allows movement inside/outside the tanks and operations are similar to the syringe. An inside movement of the piston indicate de-ballasting and an outside movement of the piston indicate ballasting. The thrust required at the piston head for the linear actuator is a function of the diameter of ballast tank and the length of ballast tanks is limited by the length of vehicles (i.e., maximum length of tank $\leq 0.15 L$).

Herein, we consider different length to diameter ratios k for the DO1 with $\pm B = 2.5, 5, 7.5$ and 10 kg. Following Tiwari and Sharma [20] the buoyancy capacity of piston-driven VBS is as follows:

$$B = \nabla \rho \eta_{vol} = (\pi/4) D_p^2 L_p \rho \eta_{vol} = (\pi/4) D_p^3 k \rho \eta_{vol} \quad (2)$$

where η_{vol} is the volumetric efficiency defined as the ratio of the volume of cylindrical ballast tank which can be filled/emptied to control the buoyancy to overall volume of the piston operated cylindrical ballast tank, ρ is the density of fluid, V is the volume of piston-driven cylindrical ballast tank, L_p and D_p are the length and diameter of the piston-driven cylindrical ballast tank respectively, and k is the length to diameter ratio of the piston. Now, the thrust required at the piston head is as follows:

$$T_{rp} = A_{cs}\Delta P/\eta_a = (\pi/4)D_p^2\Delta P/\eta_a = (\pi/4)D_p^2((\rho gh + P_{atm}) - P_{in})/\eta_a \quad (3)$$

where P_{in} is the pressure inside the ballast tank, P_{atm} is the atmospheric pressure, h is the depth of water at which VBS is designed to be operated, η_a is the linear actuator efficiency and g is the gravitational acceleration.

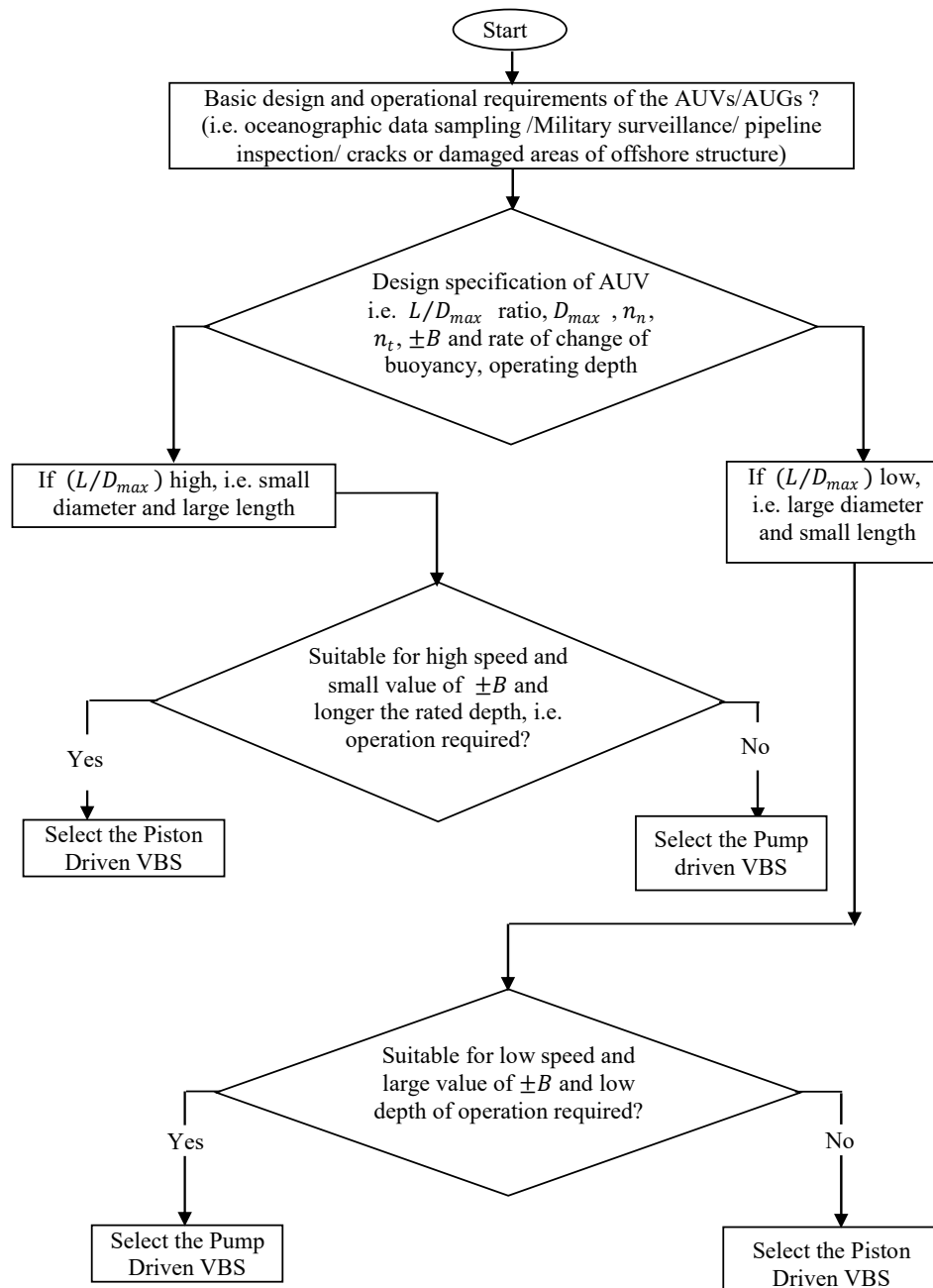


Figure 3. Our complete approach for the design and selection of the VBS.

To illustrate the implementation of Equations (2) and (3), we consider $\pm B = 2.5, 5, 7.5$ and 10 kg , and analyze different options of k and these results are presented in Figure 4a. From this it can be observed that the DO1 is suitable for large L/D_{\max} ratio of the vehicles. Assuming that the efficiency of the electric linear actuator Stock et al. [21] is at around 80 percent and the pressure inside the cylindrical ballast tank is atmospheric then the computed thrust required at the piston head versus the diameter of piston operated cylindrical ballast tank is shown in Figure 4b. We can see that for a piston diameter of 0.25 m , the thrust required at the piston head at 100 m depth is 58 kN and for the same piston diameter at the depth of 400 m it is almost 245 kN and this is very high. Also we can observe from the results that the required thrust increases non-linearly with the piston diameter and the depth of operation and these results imply that the piston-driven VBS is suitable, in terms of power consumption, to smaller operating depths and piston diameters.

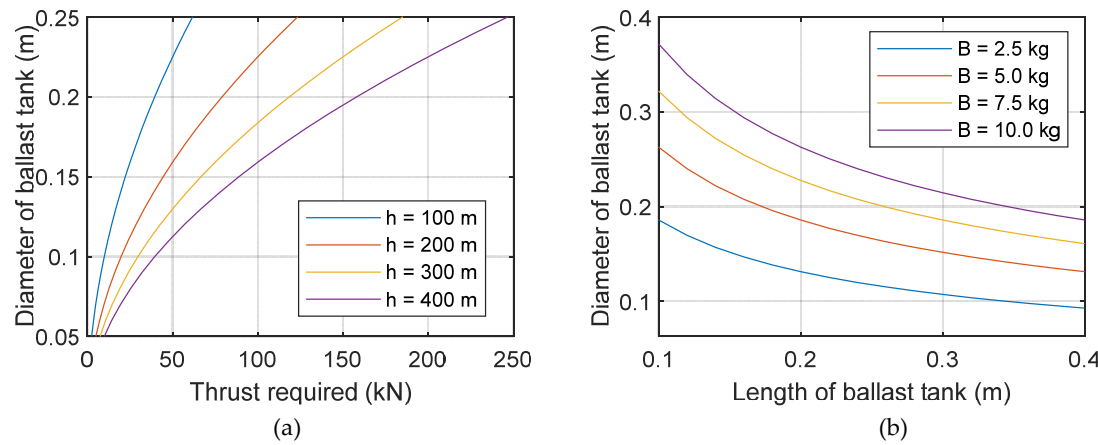


Figure 4. (a) Computed length vs. diameter of piston operated cylindrical ballast tank, (b) Thrust required at piston head vs. diameter of piston operated cylindrical ballast tank.

In the DO2—Pump-driven VBS—the components are: Ballast tank (preferably spherical), hydraulic pumps, ‘Brushless Direct Current (BLDC)’ motor, power source, and control valves, etc. An important advantage of this type of the VBS is that it can be used for the large capacity of buoyancy changes required and it is applicable in both the speeds of ascent and decent in the gliding mode the UVs. Our conceptual design approach of DO2 is shown in Figure 5 and herein we focus on the design of large capacity pump-driven VBS. Important to note pumps can classified as centrifugal pumps, i.e., Non-Positive Displacement Pump (NPDP) and Positive Displacement Pump (PDP). However, NPDP cannot be used for deep water applications because they do not ensure constant flow rate with increasing pressure, do not work at high hydrostatic pressure, are not scalable (suit only large sizes) and are noisy.

Hence, it is better to use the PDP. Furthermore, selection of type of pump for the VBS depends upon the design parameters, e.g., Mass Flow Rate (MFR) required, viscosity of the fluid to be pumped, and maximum operating pressure etc. Herein, we have chosen an external gear PDP and the related analysis and reasons are explained in Petersen and Jacoby [22]. We focus on the design of VBS for UVs operating at the depth of up to 400 m . We observe that the external gear pump is excellent for high pressure differential operation (needed for high depth of operations), and the ability to handle thin fluids.

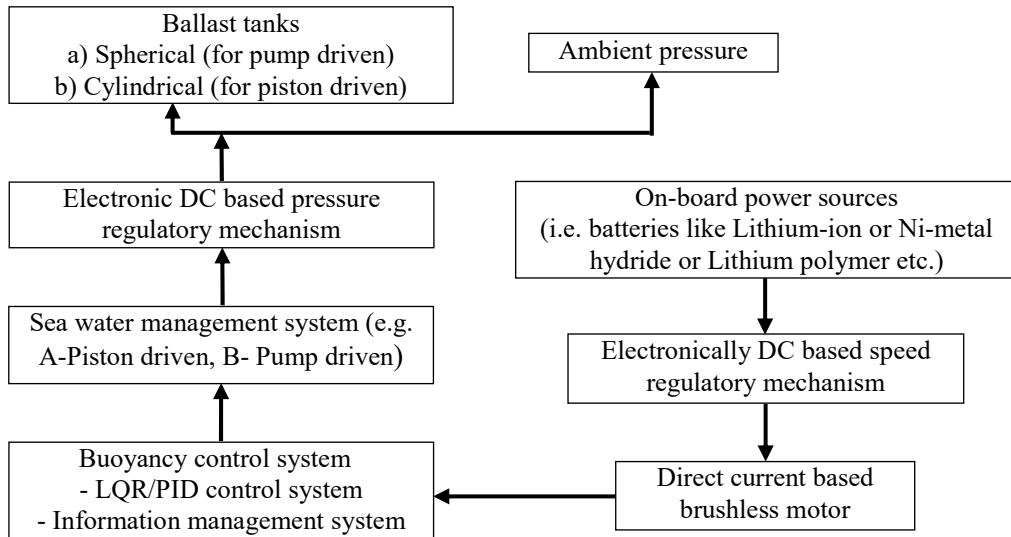


Figure 5. Our conceptual design approach of pump-driven VBS.

3.4. Module 2.1—Mass Metric Analysis of the VBS

As the basic function of the VBS is to change the buoyancy via the changes in weight it is important that it should be designed with the maximum possible ratio of change of buoyancy to net weight of the VBS, this ratio is called mass metric β and defined as follows:

$$\beta = \frac{\text{Total change in buoyancy}}{\text{Weight of the VBS}} \quad (4)$$

Hence, the weight of VBS becomes critical and the following components contribute to the weight: power source, ballast tank, PDP, BLDC motor and flow control unit such as check valve, pressure relief valve, four ways—3 position valves, two ways—2 position valve, flow direction control valve, and electronic controller unit, etc. All these components contribute in the weight but out of all the above components, weight of the VBS is mostly influenced by four components: power source, ballast tank, PDP, and BLDC motor.

The weight of ballast tank of VBS is function of the size, i.e., buoyancy capacity for which ballast tank has to be designed and the thickness t of the ballast tank which is a function of maximum pressure at which the ballast water can be taken in or taken out and the choice of material. In this study we assumed spherical ballast tank due to its best pressure resistant quality. We use the basic structural analysis with hoop stress from Raymond and Young [23] to compute the required thickness of ballast tanks and assume them to be of the thin walled spherical section. Following Raymond and Young, the hoop stress acting on the spherical vessel is as follows:

$$\sigma = \frac{pR}{2t} \quad (5)$$

Moreover, regarding strength, $\sigma \leq \sigma_u/SF$, i.e., $t \geq (pR/2\sigma_{ts})SF$, where σ is the hoop stress, R is the radius of spherical ballast tank, p is the internal pressure, t is the thickness of ballast tank, σ_u is the ultimate tensile strength of chosen material of ballast tank and SF is the safety factor. In general we use SF of 1.2 and now, the total mass of the material used for ballast tank is computed as follows:

$$\begin{aligned} M_{bt} &= \nabla_{mt}\rho_{mt} \\ &= \frac{4\pi}{3}((R_{in} + t)^3 - R_{in}^3)\rho_{mt} \end{aligned} \quad (6)$$

where $R_{in} = (0.75B/\pi\rho_m\eta_{vol})^{1/3}$, M_{bt} is the total mass of the material, ρ_m is the density of material, V_{mt} is the volume of the material used for ballast tank, R_{in} is the inner diameter of spherical ballast tank and η_{vol} is volumetric efficiency. The η_{vol} is defined as the following:

$$\eta_{vol} = \frac{\text{volume required to change the buoyancy}}{\text{volume of the designed ballast tank}} \quad (7)$$

To avoid large sloshing effects and allow sufficient expansion and contraction of fluid inside ballast tanks, we assume that the tanks are filled always in between 10 to 90%, i.e., not less than 10% and not higher than 90%. The computed masses of ballast tank with different material choices are shown in Figure 6, and are computed for three different capacities of the ballast tanks, i.e., 5, 10 and 15 kg and 0.5 cm thickness are taken. In our results on the x-axis, the m_1, m_2, \dots, m_8 represent material 1, material 2, ..., material 8 and they are: 1—High strength Steel (HY80), 2—Titanium alloy (6-4 STOA), 3—Aluminum alloy (7075-6), 4—FRP (Epoxy/S-class), 5—Acrylic, 6—PVC, 7—CFRP and 8—MMC. We observe that the maximum weight of the ballast tank of thickness 0.5 cm with 10 kg capacity, i.e., 0.1373 cubic meter capacity for material high strength steel (HY 80) is 9.7 kg and minimum for the same capacity and thickness is 1.4736 kg using the acrylic material.

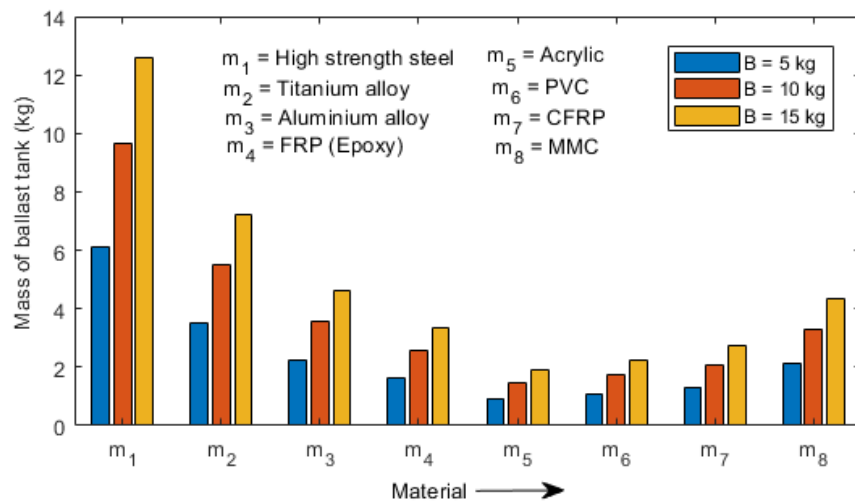


Figure 6. Material chosen vs. weight of ballast tank at thickness $t = 0.5$ cm.

We note that the weight needs to bear the hydrostatic pressure and because of this the ultimate tensile/compressive strength and Young's modulus (E) need to be of sufficient value to avoid any structural failure. Furthermore, it is important to note that the materials which are reducing the weight of the ballast tank for the same capacity and thickness may not be sustainable or may not satisfy some particular specifications of the VBS, e.g., criteria for buckling. Hence, for the ballast tanks a proper material of low density but high σ_u and E is preferred. As neither the AUVs nor the AUGs have an umbilical cable that connects them to the mother ship or a power generation system on-board, for them carrying power storage on-board becomes the only feasible option. Hence, for them, in the long range and duration of operations, the required power becomes very high and this high power storage results in a high battery weight.

This high weight affects the payload of the AUV/AUG adversely and, regarding endurance, it is important that the energy density (in Joule/kg) is kept as high as possible and it is utilized as efficiently as possible, i.e., not to be used for depth/buoyancy control operations, etc. There exist two types of batteries: Primary or secondary batteries, but more than 85 percent of the AUVs and around 70 percent of the UVs use the secondary batteries.

Regarding actual implementations, the working of VBS plays an important role in changing the buoyancy of UVs. In this regard, the basic circuit diagram of our proposed VBS is shown in Figure 7.

We note that the shaft of PDP is connected to the BLDC motor and when the pressure inside the ballast tanks is lower than the ambient pressure, then to increase the buoyancy we need to operate the VBS. For this the flow is passed from the ballast tank to the pump through C and A valves and draining the water to the sea through check valves B and D. Similarly, in order to decrease the buoyancy when the pressure inside the ballast tank is smaller than the ambient sea water pressure, then the four way-three position valve is moved to the left, i.e., disconnected from the pump and the flow is passed through two way-two position valve that is in the connected position with the ballast tank. If the ambient sea water pressure is lower than the ballast tank pressure and still we need to decrease the buoyancy, then the four way-three position valve is brought back to its right most position and the flow is passed from the ambient to D, and A to pump and then through the check valve to the ballast tank through B and C valves.

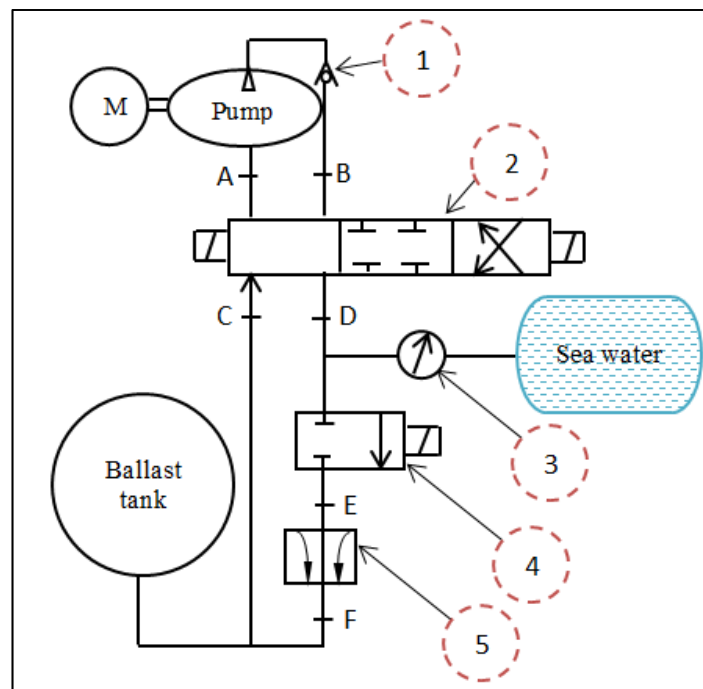


Figure 7. Basic circuit diagram of the proposed VBS: 1. check valve, 2. four way-three position valve, 3. flow rate gauge, 4. two way-two position valve and 5. flow control valve.

From our review of literature we observe that the design specification of VBS (i.e., maximum capacity of the buoyancy change, and maximum rate of buoyancy change, etc.) depend on the missions of UV and they are always mission-centric. Some of the existing $\pm B$ and \dot{m} options are listed in Table 2. To analyze the performance of our designs, we opt for the mass metric analysis, as defined in Section 3.2. Module 1.2, plays an important role in the design of VBS and it needs to be as high as possible. Total mass of the VBS is a function of the components as follows:

$$M_{vbs} = f(M_{ps}, M_{bt}, M_{pump}, \text{mass of control system, valves, sensors}) \quad (8)$$

Table 2. Listing of the existing $\pm B$ and \dot{m} options.

$\pm B$	\dot{m}	Description of VBS Design	Depth Rating	References
90 kg	9 kg/min	For shallow water operation AUVs	Up to 10 m	Tangirala and Dzielski [4]
18 kg	3 kg/min	For long cruising range AUVs	Up to 1000 m	Zhao et al. [2]
30 kg	1 kg/min	For deep ocean AUVs	Up to 6000 m	Worall et al. [11]

But the main components that contribute in the M_{vbs} are as follows:

$$M_{vbs} = M_{ps} + M_{bt} + M_{pump} + M_{motor} \quad (9)$$

where M_{ps} is the mass of power source and it is a function of the depth of operation, rate of change of buoyancy required, type of the battery (energy density) and number of cycles for which net buoyancy has to be changed; M_{bt} is the mass of the ballast tank and it is a function of the buoyancy capacity required, material used and thickness of the ballast tank; M_{pump} is the mass of the pump and it is a function of the rate of buoyancy change capacity (in cc/rev); and M_{motor} is the mass of motor and it is a function of power requirement of the pump, which is also function of the depth of operation and maximum of rate buoyancy change required. Please see Appendix A for more details on selection guidelines for battery, pump and motor. Herein, we investigate for different rate buoyancy change and accordingly present the design approach. To clearly present the design approach and show its range of applications, we consider the following design examples:

- *Design example 1:* Herein, we consider the VBS of $\pm B = 5$ kg, $t = 0.5$ cm and power source (secondary batteries) = 2.88 MJ. As has been observed before the capacity, material and thickness of material plays an important role for computing the weight of ballast tank of VBS. As before, we consider m_1, m_2, m_3, m_4, m_5 and m_6 and the secondary battery options are: Lithium-ion (CGR-18650HG), Ni-metal hydride and Lithium polymer. The pumps of capacities 5.1, 6.0 and 8.2 cc/rev and operating speed of 1800 RPM are considered. Our analysis is based upon 1800 rpm of the pump, but it can vary in between 700 to 3000 rpm and this can be used to control the rate of change of buoyancy. For $\pm B = 5$ kg, the computed β of VBS versus different rates of change of buoyancy for different options of the batteries are shown in Figure 8a. In which a particular rate of change of buoyancy corresponds to a specific pump capacity and rpm.

- *Design example 2:* Herein, we consider the VBS of $\pm B = 10$ kg and other parameters are kept as the same of Design example 1. For $\pm B = 10$ kg, the computed β of VBS versus different rates of change of buoyancy for different options of the batteries are shown in Figure 8b.

- *Design example 3:* Herein, we consider the VBS of $\pm B = 15$ kg and other parameters are kept as the same of Design example 1. For $\pm B = 15$ kg, the computed β of VBS versus different rates of change of buoyancy for different options of the batteries are shown in Figure 8c. Now, from the presented results of Figure 8, we observe the following:

- For a good design, the β needs to be maximized. Our results in Figure 8a–c indicate that for the design B of 15 kg, the Ni-metal hydride battery with m_5 material offers the highest β and it is also closely similar for the option of Lithium polymer battery with m_5 material. But the performance is lower for the option of Lithium ion.

- Depending upon the selected material for ballast tank, design's performance can change drastically. In fact it can change from non-feasible to feasible and we state here that for any feasible design of the VBS the $\beta > 1$, e.g., note that in Figure 8c $\beta > 1$ for all except one.

- It is observed that a design for B of 15 kg will not be feasible at lower B because the tank weight will be higher even if the same pump is used. Figure 8a indicates that none of designs are feasible, even for all options of material selected for the ballast tank and batteries.

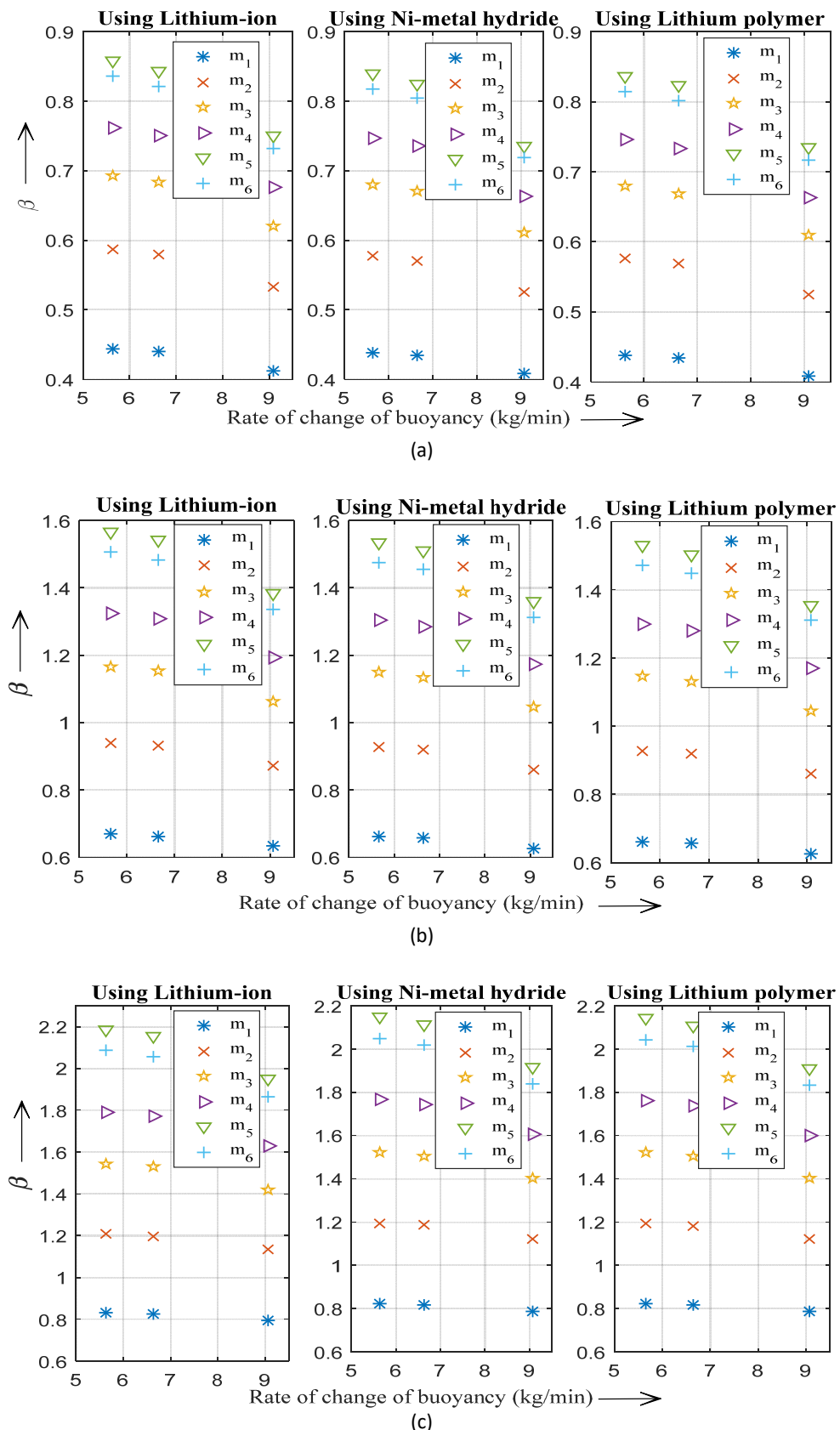


Figure 8. (a) Rate of change of buoyancy vs. weight of VBS for $B = 5\text{ kg}$, (b) Rate of change of buoyancy vs. weight of VBS for $B = 10\text{ kg}$ and (c) Rate of change of buoyancy vs. weight of VBS for $B = 15\text{ kg}$.

4. Integrated Design and Analysis of the AUV, VBS and Controller

4.1. Module 2.2—Mathematical Modeling of the Dynamics of AUV and Its Integration with the VBS

Herein, we analyze the operation and behavior of AUV in an integrated environment with the VBS. Most of the existing AUVs use the vertical thrusters to dive down and/or for vertical motion, but this is not power efficient and in this regard the VBS is an alternative technology that allows both the operations of diving down and/or for vertical motion without thruster. The list of the notations used for mathematical modeling of the dynamics of AUV and its integration with the VBS are reported in Table 3.

Table 3. List of the notations used in six degrees of freedom (DOF).

S. No.	Translation	Translational Force Components	Linear-Velocities	Positions
4	Roll	Moment about x -axis, K	p	ϕ
5	Pitch	Moment about y -axis, M	q	θ
6	Yaw	Moment about z -axis, N	r	ψ
1	Surge	Force in the surge direction, X	u	x
2	Sway	Force in the sway direction, Y	v	y
3	Heave	Force in the heave direction, Z	w	z

Following the study of general six degrees of freedom (DOF) for any UV can be analyzed in two co-ordinate reference frames and they are:

- Body Fixed Frame (BFF): It is the local co-ordinate system for the UV and all the UV's motions etc. are defined in the BFF. This is defined as a moving coordinate fixed with the vehicle and denoted by (X_B , Y_B , Z_B) where X_B , Y_B and Z_B are the longitudinal, transverse and normal axes. Here, the origin of the BFF is chosen such that it falls on the center line of UV and at the center of all three directions, i.e., middle of the body.

- Earth Fixed Frame (EFF): This is Euler's frame of reference and it is inertial/global co-ordinate system and it is defined as (X_E , Y_E , Z_E) and both the BFF and EFF are shown in Figure 9.

Now, in reference to Figure 9, and following [24] the dynamical governing Equations are as follows:

$$\eta = [\eta_1, \eta_2]^T; v = [v_1, v_2]^T; \tau = [\tau_1, \tau_2]^T, \eta_1 = [x, y, z]; v_1 = [u, v, w]; \tau_1 = [X, Y, Z] \quad (10)$$

$$\eta_2 = [\phi, \theta, \psi]; v_2 = [p, q, r]; \tau_2 = [K, M, N], \dot{\eta} = [\dot{\eta}_1, \dot{\eta}_2]; \dot{\eta}_1 = J_1(\eta_2)v_1; \dot{\eta}_2 = J_2(\eta_2)v_2 \quad (11)$$

where η_1 , η_2 , η , $\dot{\eta}_1$, $\dot{\eta}_2$ and $\dot{\eta}$ are the position vector, orientation vector, combined position and orientation vectors, the rate of change of position vector, rate of change of orientation vector and combination rate of change of both position and orientation vectors, respectively in the EFF. Also, v_1 , v_2 , v , τ_1 , τ_2 and τ are the linear velocity, angular velocity, combined linear and angular velocity vector, linear force, moment and combined linear force and moment vectors, respectively in BFF. Then, the kinematic Equations in vector form are as follows:

$$\begin{pmatrix} \dot{\eta}_1 \\ \dot{\eta}_2 \end{pmatrix} = \begin{pmatrix} J_1(\eta_2) & 0 \\ 0 & J_2(\eta_2) \end{pmatrix} \begin{pmatrix} v_1 \\ v_2 \end{pmatrix} \quad (12)$$

where $J_1(\eta_2)$ and $J_2(\eta_2)$ are the rotational (transformation) matrices. We note that the $J_1(\eta_2)$ is a skew-symmetric matrix and it can be written as follows:

$$J_1(\eta_2) = \begin{bmatrix} c\psi c\theta & -s\psi c\phi + c\psi s\theta s\phi & s\psi s\phi + c\psi c\phi s\theta \\ s\psi c\theta & c\psi c\phi + s\theta s\psi s\phi & -c\psi s\phi + s\theta s\psi c\phi \\ -s\theta & c\theta s\phi & c\theta c\phi \end{bmatrix}, \text{ and } J_2(\eta_2) = \begin{bmatrix} 1 & s\phi t\theta & c\phi t\theta \\ 0 & c\phi & -s\phi \\ 0 & s\phi/c\theta & c\phi/c\theta \end{bmatrix} \quad (13)$$

where s represents sine function, c represents cosine function and t represents tangent function. Equations (12) can be compactly re-written as $J = [J_1(\eta_2), J_2(\eta_2)]^T$.

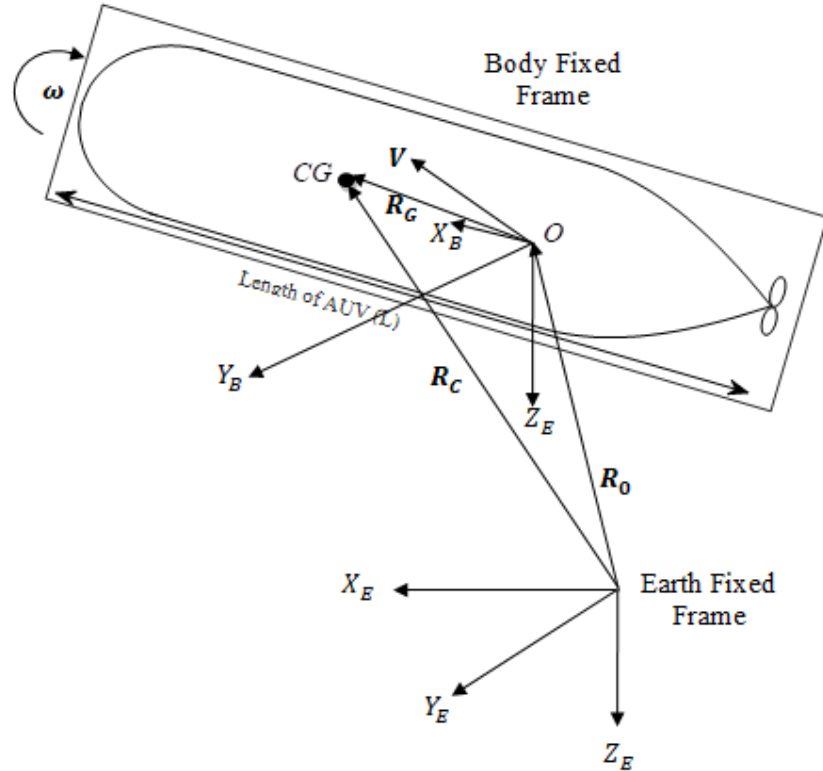


Figure 9. Schematic description about the reference planes—Body Fixed Frame (BFF) and Earth Fixed Frame (EFF).

Similarly, following [25,26] the dynamic equations of motion in vertical planes are as follows:

$$Z = m[(\dot{w} + v p - u q) + (\dot{p} y_G - \dot{q} x_G) + p r x_G + q r y_G - z_G(p^2 + q^2)] \quad (14)$$

$$\begin{aligned} M = I_y \dot{q} + (I_x - I_z)r p + (q p - \dot{r})I_{yz} + (p^2 - r^2)I_{zx} - (\dot{p} + q r)I_{xy} \\ + m[(\dot{u} - v r + w q) \times z_G - (\dot{w} + v p - u q) \times x_G] \end{aligned} \quad (15)$$

where I_x , I_y and I_z are moment of inertia about X_B , Y_B and Z_B respectively, I_{xy} , I_{yz} and I_{zx} are product of inertia and the other terms are same as defined in Table 3. Herein, we analyze the operation and behavior of an AUV which is integrated with the designed VBS. Most of contemporary AUVs have the vertical thrusters to dive down or come up in the vertical motion, but they are highly power inefficient. A VBS is an alternative of that in addition with minimum possible energy consumption. The stability in vertical motion involves heave and pitch motions and the surge is coupled with pitch and heave motions through the meta-centric height (z_G). The dynamic coupling can be included in the hydrodynamic coefficient with respect to vehicle's CoG (x_G , y_G , z_G) instead of its geometric center (x_B , y_B , z_B). Using these observations, we make the following standard assumptions:

- We focus only on the heave motion, i.e., motion of the UV is confined to only the vertical plane resulting into: $p, \dot{p}, r, \dot{r}, v, \dot{v}, \phi, \psi = 0$.

- Surge velocity is constant in the heave and pitch DOF resulting into: $\dot{u} = 0$.
- UV is neutrally buoyant with half-filled ballast tanks.

Further assuming that θ to be very small, then the kinematic and dynamic Equations in vertical plane get simplified and written as follows:

$$\dot{\theta} = q \text{ and } \dot{z} = -u\theta + w \quad (16)$$

$$Z = m(\dot{w} - uq - x_G\dot{q}), \quad (17)$$

$$M = I_y\dot{q} - mx_G(\dot{w} - uq) \quad (18)$$

Then, we sum all the external forces and moments acting on the UV that are influencing the motion of UV in the vertical plane, i.e., components of the drag, control surface, hydrodynamic forces, gravity and buoyancy, etc. Addition of these to the forces and moments due to the VBS results in two different equations as follows:

$$\begin{aligned} \sum Z &= Z(q, \dot{q}, w, \dot{w}, \delta) + Z_g - Z_{drag} + Z_{weight \ of \ BT} \\ &= Z''_q Uq + Z''_{\dot{q}} \dot{q} + Z''_w Uw + Z''_{\dot{w}} \dot{w} + Z''_{\delta} U^2 \delta - 0.5\rho \int_{nose}^{tail} C_d b(x)(w - qx)|w - qx| dx \\ &\quad + (W - B)\cos \theta + (dw_1 + dw_2)\cos \theta \end{aligned} \quad (19)$$

$$\begin{aligned} \sum M &= M(q, \dot{q}, w, \dot{w}, \delta) + M_g - M_{drag} + M_{weight \ of \ BT} \\ &= M''_q Uq + M''_{\dot{q}} \dot{q} + M''_w Uw + M''_{\dot{w}} \dot{w} + M''_{\delta} U^2 \delta + (x_G W - x_B B) \cos \theta - (z_G W - z_B B) \sin \theta \\ &\quad + \frac{\rho}{2} \int_{nose}^{tail} C_d b(x)(w - qx)|w - qx| dx + (-L_1 dw_1 + L_2 dw_2) \end{aligned} \quad (20)$$

where U is the forward speed of the vehicle and L_1, L_2 are the distances between the CoG of the AUV and CoG of the nose and tail ballast tanks, respectively. And dw_1, dw_2 are changes in the weight of the nose and tail ballast tanks respectively, C_d is the drag coefficient and $b(x)$ is diameter of the UV at any locations x along the length of the vehicle from nose to tail. Herein, we present the design and implementation of VBS and it can be used to glide and hover at a depth of/up to 400 m without the application of vertical thrusters, and at a low forward speed of 0.02 m/s. Additionally it can be used for grounding the UV with low energy consumption. It is known that the control surfaces are effective and efficient only at the high speed of UV and because of this we can neglect the effect of control surfaces, for more details see Leo et al. [27]. This results in the linear forms of Equations (19) and (20) and balanced these with Equations (17) and (18), finally can be written as follows:

$$(m - Z''_{\dot{w}})\dot{w} - (mx_G + Z''_{\dot{q}})\dot{q} = Z''_w U w + (Z''_q + m) U q + (W - B) + (dw_1 + dw_2) \quad (21)$$

$$-(mx_G + M''_{\dot{w}})\dot{w} + (I_y - M''_{\dot{q}})\dot{q} = -(z_G W - z_B B) \theta + M''_w U w + (M''_q - mx_G) U q + (L_2 dw_2 - L_1 dw_1) \quad (22)$$

Buoyancy of the UV is controlled by either filling or emptying of the ballast tanks, i.e., by changing the weight of the UV. This results in the weight control of UV using the pump mass flow rate and mathematically it is written as follows:

$$d\dot{w}_1 = f_{r1} \text{ and } d\dot{w}_2 = f_{r2} \quad (23)$$

where $d\dot{w}_1$, $d\dot{w}_2$ are the rate of change of weight of water inside the ballast tank 1 and ballast tank 2, respectively; f_{r1} , f_{r2} are the flow rate of pump 1 and pump 2, respectively; and these are functions of the speed of motor, i.e.,:

$$f_{r1} = Q \times \rho \times g \times N_1 \text{ and } f_{r2} = Q \times \rho \times g \times N_2 \quad (24)$$

where Q , ρ and g are the pump flow rate capacity (in cubic meter per revolution), sea water density (in kg/m^3) and gravitational acceleration (in m/sec^2), respectively; and N_1, N_2 are the speed of motor (in RPM) for the nose and tail ballast tanks, respectively. Furthermore the technical specifications of VBS used for simulation in this study are shown in Table 4a and the state-space Equation for the motion of UV, which is integrated with the VBS in the vertical plane, can be written using Equations (16), (21–23) and it is as follows:

$$\begin{aligned} & \left(\begin{array}{cccccc} 1 & 0 & 0 & 0 & 0 & 0 \\ 0 & (m - Z''_{\dot{w}}) & -(mx_G + Z''_{\dot{q}}) & 0 & 0 & 0 \\ 0 & -(mx_G + M''_{\dot{w}}) & (I_y - M''_{\dot{q}}) & 0 & 0 & 0 \\ 0 & 0 & 0 & 1 & 0 & 0 \\ 0 & 0 & 0 & 0 & 1 & 0 \\ 0 & 0 & 0 & 0 & 0 & 1 \end{array} \right) \begin{pmatrix} \dot{\theta} \\ \dot{w} \\ \dot{q} \\ \dot{z} \\ d\dot{w}_1 \\ d\dot{w}_2 \end{pmatrix} \\ &= \left(\begin{array}{cccccc} 1 & 0 & 0 & 0 & 0 & 0 \\ 0 & Z''_w U & (Z''_q + m)U & 0 & 1 & 1 \\ -(z_G - z_B)W & M''_w U & (M''_q - mx_G)U & 0 & -L_1 & L_2 \\ -U & 0 & 0 & 0 & 0 & 0 \\ 0 & 0 & 0 & 0 & 0 & 0 \\ 0 & 0 & 0 & 0 & 0 & 0 \end{array} \right) \begin{pmatrix} \theta \\ w \\ q \\ z \\ dw_1 \\ dw_2 \end{pmatrix} + \begin{pmatrix} 0 & 0 \\ 0 & 0 \\ 0 & 0 \\ 0 & 0 \\ 1 & 0 \\ 0 & 1 \end{pmatrix} \begin{pmatrix} 0 \\ 0 \\ 0 \\ 0 \\ f_{r1} \\ f_{r2} \end{pmatrix} \end{aligned} \quad (25)$$

where the hydrodynamic coefficients are as follows:

$$\begin{aligned} Z''_{\dot{q}} &= Z'_q \times a_4, Z''_{\dot{w}} = Z'_{\dot{w}} \times a_3, Z''_q = Z'_q \times a_3, Z''_w = Z'_{\dot{w}} \times a_2, M''_{\dot{q}} = M'_q \times a_5, \\ M''_{\dot{w}} &= M'_{\dot{w}} \times a_4, M''_q = M'_q \times a_4, M''_w = M'_{\dot{w}} \times a_3, Z''_{\delta} = Z'_{\delta} \times a_2, M''_{\delta} = M'_{\delta} \times a_3 \end{aligned} \quad (26)$$

$$Z_{\dot{q}} = \frac{\partial Z}{\partial \dot{q}}, Z_q = \frac{\partial Z}{\partial q}, Z_{\dot{w}} = \frac{\partial Z}{\partial \dot{w}}, Z_w = \frac{\partial Z}{\partial w}, M_{\dot{q}} = \frac{\partial M}{\partial \dot{q}} \quad (27)$$

$$M_q = \frac{\partial M}{\partial q}, M_{\dot{w}} = \frac{\partial M}{\partial \dot{w}}, Z_{\delta} = \frac{\partial Z}{\partial \delta}, M_{\delta} = \frac{\partial M}{\partial \delta}, M_w = \frac{\partial M}{\partial w} \quad (28)$$

where Z'_q , $Z'_{\dot{w}}$, Z'_q , $Z'_{\dot{w}}$, M'_q , $M'_{\dot{w}}$, M'_q , $M'_{\dot{w}}$, Z'_{δ} and M'_{δ} are the non-dimensional hydrodynamic parameters and $a_2 = 0.5 \times \rho \times L^2$, $a_3 = 0.5 \times \rho \times L^3$, $a_4 = 0.5 \times \rho \times L^4$ and $a_5 = 0.5 \times \rho \times L^5$.

Table 4. (a) Technical Specifications of VBS (b) Input and Output Design Parameters of CSM for the Design of VBS.

(a)		
Capacity of Pump (Q)	8.2 cc/rev	
Efficiency	0.60	
Buoyancy capacity ($\pm B$)	100 N	
Depth rating	400 m	
Maximum operating speed	1800 RPM	
Rate of change	9 kg/min @ 400m	
Power consumption of motor	0.92 kw @ 400 m	

(b)		
Parameter	Description	Values
ρ	Density of sea water	1025 kg/m ³
W	Weight	2989.3 N
m	Mass	304.7228 kg
B	Buoyancy	304.7228 kg
L	Characteristic length	2.8 m
I_{xx}	Mass M.O.I. about x-axis	7.5 kg-m ²
I_{yy}	Mass M.O.I. about y-axis	133 kg-m ²
I_{zz}	Mass M.O.I. about z-axis	133 kg-m ²
x_G	x-coordinate of CG from origin	0 m
y_G	y-coordinate of CG from origin	0 m
z_G	z-coordinate of CG from origin	0.012 m
x_b	x-coordinate of CB from origin	0 m
y_b	y-coordinate of CB from origin	0 m
z_b	z-coordinate of CB from origin	0 m

4.2. Module 3.1—Designed Parameters of AUV

As shown in Figure 10, the CoG of nose side ballast tank is L_1 meter and of the tail side ballast tank is L_2 meter from the CoG of the AUV. We take the L_1 as slightly higher than L_2 because it results in an economic control mechanism as the differential fluid movement along with same rpms of the PDPs allow us to control trim and pitch. Herein, we restrict the difference to less than 20% as the higher difference will result into larger trim and pitch while making the vehicle unstable. Initially the ballast tanks are half-filled, i.e., neutrally buoyant AUV. And, when both the ballasts tanks are filled or emptied at the same rate of change of buoyancy to increase or decrease the buoyancy of the vehicle, it also pitch up or pitch down respectively. Here, we note that for diving and hovering operations in general, small trim and pitch are always preferred, but not too large. In this study of computer simulation model the CoG of nose side ballast tank L_1 is 0.7 m, CoG of tail side ballast tank L_2 is 0.6 m, L_n , L_m , L_t , r_n and r_t are 0.56 m, 1.51 m, 0.72 m, 3 and 2 respectively. The L/D ratio is 7.

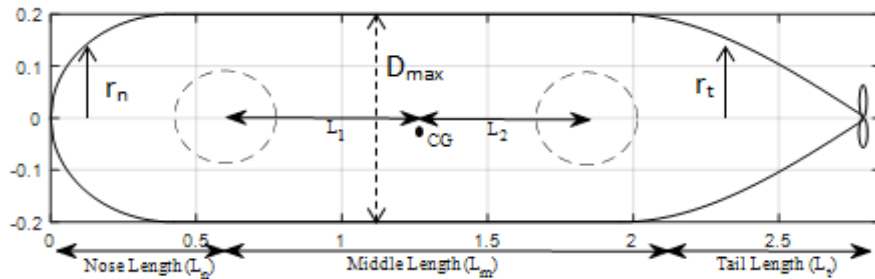


Figure 10. Modular form of AUV integrated with VBS for CSM.

Important inertial properties, including the location of mass center, and geometric center etc., are listed in Table 4b. Depth control algorithm of the AUV is designed both in open loop system and closed loop system, using the LQR controller. This LQRC is used to study and demonstrate the hovering ability and the implementation has been done with the MatlabTM using its simulink module and the designed simulink structure of our computer simulation model (CSM) is shown in Figure 11.

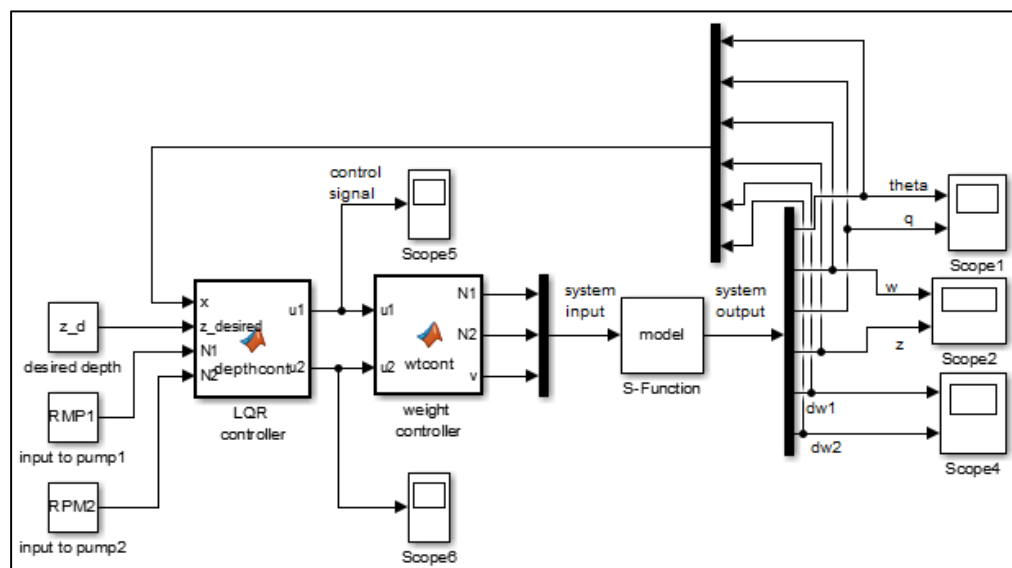


Figure 11. Simulink structure of the Linear Quadratic Controller (LQR) controller used in our CSM.

4.3. Module 3.2—Controller Design

Here, LQR controller is used to control both the heave velocity and pitch/trim of the vehicle. For these there are two inputs: One from each VBS. This results in the problem of Multiple Input and Multiple Output (MIMO) and since the LQR controller is suitable for MIMO problem we use it in our work. Now, following [28,29] we consider continuous time linear system as follows:

$$\dot{x} = Ax + Bu_{in} \quad (29)$$

where A is the state matrix, B is the input matrix, x is the state vector, and u_{in} is the input vector. Here, the objective is to design the state-feedback controller: $u_{in} = -K_c x$ where K_c is the optimal feedback control gain matrix which minimizes the infinite horizon quadratic cost function (J) defined as follows:

$$J(x, u_{in}) = \int_0^{\infty} (x^T Q x + u_{in}^T R u_{in}) dt \quad (30)$$

where Q is the positive-definite state weighing matrix and R is the positive definite energy weighing matrix which determine the relative importance of state error and expenditure of the energy respectively. To minimize the cost function (J), the closed loop optimal control gain matrix K_c is defined as follows:

$$K_c = -R^{-1}B^T S \quad (31)$$

where B and R is same as defined before and S can be computed by solving Matrix Algebraic Riccati Equation (MARE) given as follows:

$$A^T S + S A - S B R^{-1} B^T S + Q = 0 \quad (32)$$

Further it is noted that S must be a positive definite matrix for stable system and the stability of the system can be checked by computing the eigen value of $(A - BK_c)$, and if the real part of the eigen value is negative the system is stable else unstable. We implement the above mentioned formulation of the LQR controller in Matlab™ to compute the state feedback optimal controller gain matrix and to check the stability of the system.

5. Simulation Results and Discussion

5.1. Module 4.1—Conceptual Design and Simulation Results—Open Loop LQR Controller

In-take of water to both the ballast tanks without feedback control in order to increase the weight is shown in Figure 12a and it indicates that in both the ballast tanks weight increases but with a time lag of around 6 s (more clearly shown in Figure 13a as zoomed part of the same). This simulation is highly realistic because we indicate the difference clearly in terms of time lag and achieve this by operating the pumps at different RPM, i.e., motor for pump 1 (MP1) is rotating at a speed of 1600 RPM and motor for the pump 2 (MP2) is rotating at 1800 RPM. We compute all the results for a forward velocity of 0.02 m/s and the variations of the pitch angle with time in open loop in shown in Figure 12b, heave velocity with time is shown in Figure 12c depth with time is shown in Figure 12d. The heave velocity in open loop more closely observed from Figure 13b that until the ballast tanks are completely filled the vehicle is velocity is non-linear with time and after the ballast tanks are completely filled the pump is in the off mode and the vehicle achieves a terminal velocity of 0.4 m/s and depth changes continuously with a constant pitch angle of almost 7 degree.

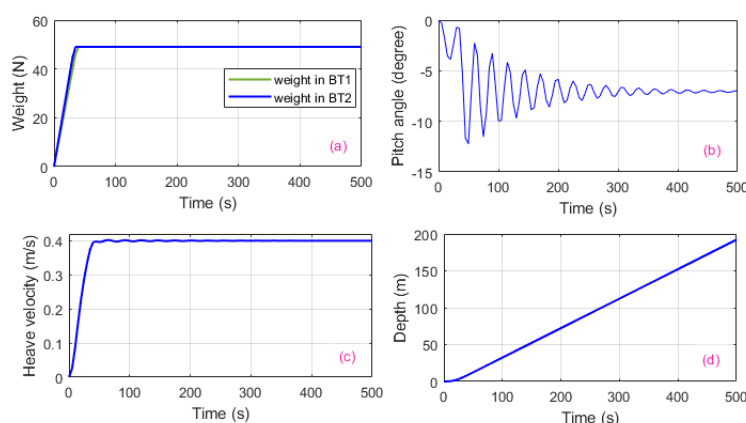


Figure 12. (a) Variation of the weight vs. time in both ballast tanks, (b) Variation of pitch angle with time, (c) Variation of sinking (heave) velocity with time and (d) Variation of depth with time in open loop.

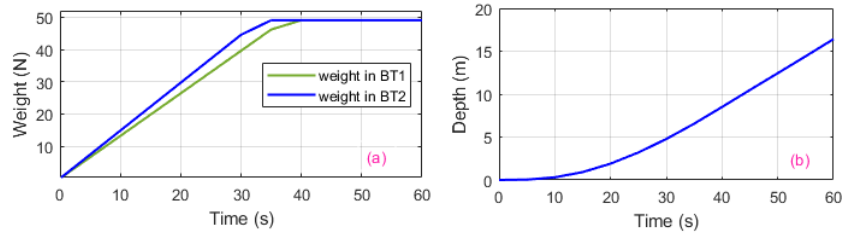


Figure 13. (a) Zoomed part of variation of the weight vs. time in both ballast tanks and (b) variation of depth with time in open loop.

5.2. Module 4.2—Conceptual Design and Simulation Results: Closed Loop LQR Controller

Here, we consider the depth control with a LQR controller. Results are presented and analyzed in combination of both open and closed loops. Non-dimensional hydrodynamic coefficients adapted from [30] and other parameters are defined in Table 4, are used to compute the optimal controller gain matrix of the system presented in Equation (25). The state matrix A and input matrix B of the system is computed shown in Equation (33) and state weighing matrix Q and energy weighing matrix R is presented in Equation (34) and these are as follows:

$$A = \begin{pmatrix} 0 & 0 & 1 & 0 & 0 & 0 \\ 0.0031 & -0.048 & -0.0064 & 0 & 8.03 \times 10^{-4} & 6.94 \times 10^{-4} \\ -0.0528 & 0.022 & -0.0134 & 0 & -0.0011 & 7.96 \times 10^{-4} \\ -0.020 & 1 & 0 & 0 & 0 & 0 \\ 0 & 0 & 0 & 0 & 0 & 0 \\ 0 & 0 & 0 & 0 & 0 & 0 \end{pmatrix} \text{ and } B = \begin{pmatrix} 0 & 0 \\ 0 & 0 \\ 0 & 0 \\ 0 & 0 \\ 824 \times 10^{-6} & 0 \\ 0 & 824 \times 10^{-6} \end{pmatrix} \quad (33)$$

$$Q = \begin{pmatrix} 3 \times 10^3 & 0 & 0 & 0 & 0 & 0 \\ 0 & 1 & 0 & 0 & 0 & 0 \\ 0 & 0 & 1 & 0 & 0 & 0 \\ 0 & 0 & 0 & 9 \times 10^3 & 0 & 0 \\ 0 & 0 & 0 & 0 & 6 \times 10^3 & 0 \\ 0 & 0 & 0 & 0 & 0 & 6 \times 10^3 \end{pmatrix} \text{ and } R = \begin{pmatrix} 5 \times 10^2 & 0 \\ 0 & 5 \times 10^2 \end{pmatrix} \quad (34)$$

- Regarding the real operations, high pitch angles are not preferred because they affect the stability and safety in the grounding/hovering operations at specific depth. To avoid, these high pitch angles we use proper the weight-ages of Q for the pitch angle and desired depth. Now, the control law used as follows:

$$u_{in} = -K_c(x - x_{desired}) \quad (35)$$

where $x_{desired}$ is the desired state vector of operation and the optimal feedback control gain matrix K_c is computed as follows:

$$K_c = \begin{pmatrix} 0.371 & 53.049 & 2.160 & 2.518 & 9.514 & 5.006 \\ 0.345 & 50.156 & 2.045 & 2.378 & 5.006 & 8.996 \end{pmatrix} \quad (36)$$

Further to check the stability of the system, eigen values of $(A - BK_c)$ are computed and since all the real parts of these are found negative as shown in Table 5, the system is concluded to be stable.

Table 5. Computed eigen values for stability analysis of the system.

Eigen Values of $(A - BK_c) =$	-0.0074 + 0.2299i -0.0074 - 0.2299i -0.0464 + 0.0000i -0.0059 + 0.0054i -0.0059 - 0.0054i -0.0035 + 0.0000i
--------------------------------	--

Now, in the closed loop the performance results of the vehicle are obtained by implementing above mentioned control law. Figure 14a indicates the variation of weight of the water with time in both the ballast tanks in the close loop operation. Initially we take water into both the ballast tanks in open loop at 1800 RPM of motor speed (i.e., resulting in 9 kg/min rate of change of buoyancy) and then after the complete filling of the ballast tanks the vehicle achieves a terminal (sinking) velocity of 0.4 m/s. Once the vehicle achieves a terminal (sinking) velocity then the pump gets off and the flow control valve is closed for short duration, i.e., till the vehicle sinks to the desired depth.

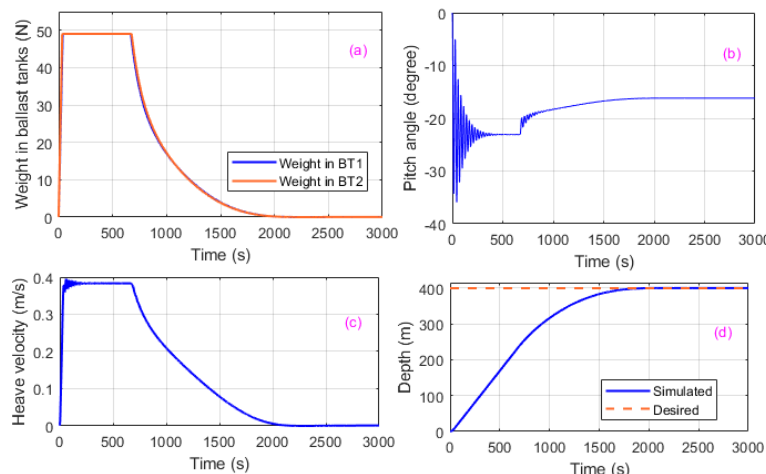


Figure 14. (a) Variation of the weight vs. time in both ballast tanks, (b) Variation of pitch angle with time, (c) Variation of sinking (heave) velocity with time and (d) Variation of depth with time in closed loop.

Later, in the control loop, the water from the ballast tanks can be removed to the half-filled state to achieve the neutral buoyancy. Variation of pitch angle with time in close loop is shown in Figure 14b, sinking (heave) velocity with time are shown in Figure 14c and depth versus time are shown in Figure 14d in closed loop operation. These results indicate that the pitch angle is around 16 degrees after reaching the desired depth. And also it can be observed that there is almost zero overshoot and no undesired oscillations of the vehicle during the process to achieve the desired depth of 400 m and the sinking (heave) velocity becomes zero as expected during the hovering at that particular depth. In order to hover at that position we assume that either the forward thruster does not exist or it is off to ensure the zero forward velocity of the vehicle.

In order to indicate the robustness of controller design, we investigate variations in state weighing and energy weighing matrices. These details are listed in Table 6. With the values of state weighting matrix from Table 6, Figure 15a indicates the variation of weight with time in ballast tanks, Figure 15b indicates the variation of pitch angle with time, Figure 15c indicates the variation of sinking (positive heave) velocity with time and Figure 15d indicates the variation of depth with time in closed loop. We can observe from these results that as the numerical values of state weighting matrix's elements increase, slight changes of the states can be noted. Nevertheless, these slight changes are only for a very short duration and the final desired depth is achieved smoothly without any high oscillations and

overshoots. Again, with the values of energy weighting matrix from Table 6, Figure 15a indicates the variation of weight with time in ballast tanks, Figure 15b indicates the variation of pitch angle with time, Figure 15c indicates the variation of sinking (positive heave) velocity with time and Figure 15d indicates the variation of depth with time in the closed loop condition.

Table 6. Details of weighing matrices used for robustness analysis.

S. No.	Parameters
1	$Q_1 = 1.25 Q$
	$Q_2 = 1.50 Q$
2	$R_1 = 1.25 R$
	$R_2 = 1.50 R$

Nomenclature: Q and R are same weighing matrices as defined before.

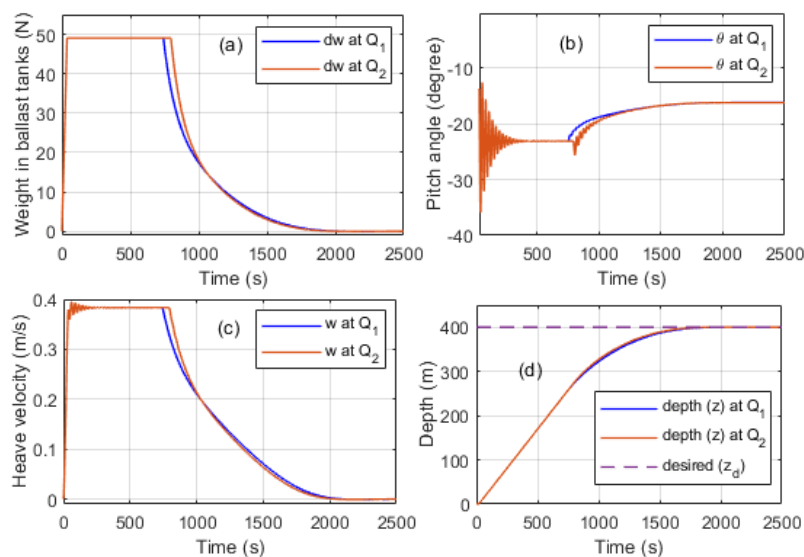


Figure 15. (a) Variation of the weight vs. time in ballast tanks, (b) pitch angle with time, (c) sinking (heave) velocity with time and (d) depth with time in closed loop for two different state weighing matrices.

As before, we can observe from these results that as the numerical values of state energy matrix's elements increase, slight changes of the states can be noted. Nevertheless, these slight changes are only for a very short duration and the final desired depth is achieved smoothly without any high oscillations and overshoots. Additionally, we note that the least pitch oscillation is achieved at around 750 s and final steady state of pitch angle is 16.5 degree at 2000 s and desired depth is achieved without any overshoot.

Now, through the results of Figures 15 and 16 we can conclude that the system is robust. We also note that the experimental investigations will be needed to support the numerical simulation results and in real world the uncertainties of environment will be influencing parameters.

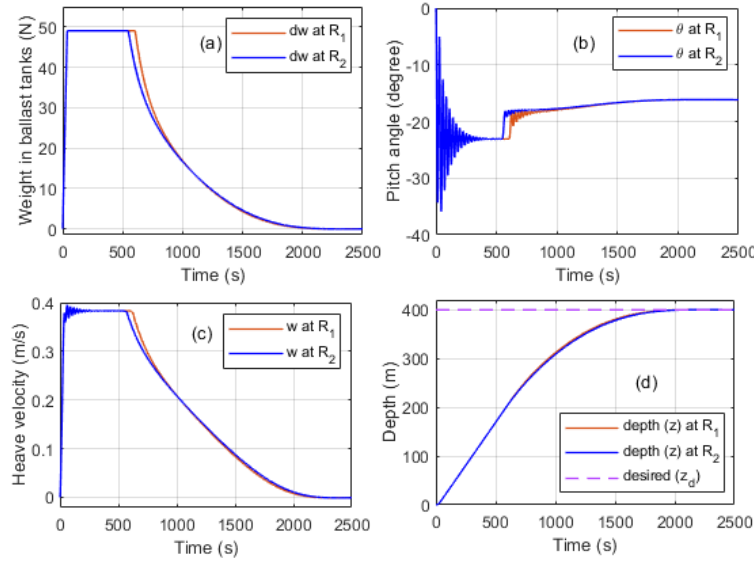


Figure 16. (a) Variation of the weight vs. time in ballast tanks, (b) pitch angle with time, (c) sinking (heave) velocity with time and (d) depth with time in closed loop for two different energy weighing matrices.

Furthermore, to ensure design scalability we present overall three design example. Details are the following:

- Design Example 1 (DE1): This has been presented in all the above mentioned results of Figures 12–14. It has been presented in full details.
- Design Examples 2 and 3 (DE2 and DE3): Two additional design examples are also investigated. To keep the manuscript of reasonable length, only design summaries along with brief discussion have been presented for DE2 and DE3. Here the lengths of AUV are 4.0 m and 5.0 m. Other details are listed in Table 7.

Table 7. Detail design parameters of AUV with integrated buoyancy system.

S. No.	Parameter	Design Example 2 (DE2)	Design Example 3 (DE3)
1	Length (m)	4	5
2	L/D ratio	7	7
3	Nose length (m)	0.8	1.0
4	Middle Length (m)	2.2	2.75
5	Tail Length (m)	1.0	1.25
6	Nose radius coefficient (r_t) *	3	3
7	Tail radius coefficient (r_t) *	2	2
8	Volume Displaced by the vehicle	0.8660	1.6926
9	Mass of the vehicle when neutrally buoyant condition (kg)	888	1735

* Note: L/D ratio, shape parameters like nose and tail radius coefficients are same for all the design examples, DE1, DE2 and DE3. Further details about the shape generation can be found in [31].

These examples indicate clearly the scalability of presented design approach. Performance of each of AUV's which is integrated with two buoyancy systems is investigated for the buoyancy capacity of 20 kg and 30 kg respectively. Other systems like pump, motor and rate of change of buoyancy have been kept same. We present the design summaries in Figures 17 and 18. Figure 17a indicates variation of the weight with time in ballast tanks, Figure 17b indicates variation of the pitch angle with

time, Figure 17c indicates variation of the sinking (positive heave) velocity with time and Figure 17d indicates variation of the depth with time in the closed loop condition for the 4 m length AUV.

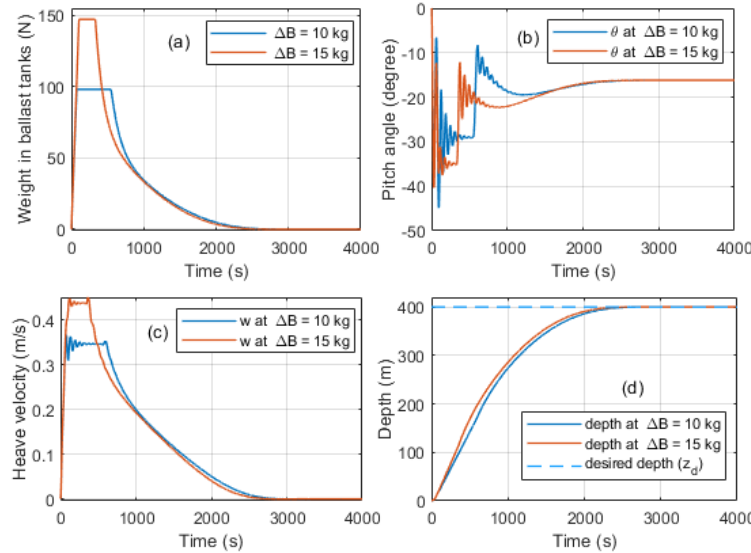


Figure 17. (a) Variation of the weight vs. time in ballast tanks, (b) pitch angle with time, (c) sinking (heave) velocity with time and (d) depth with time in closed loop for 4 m length AUV.

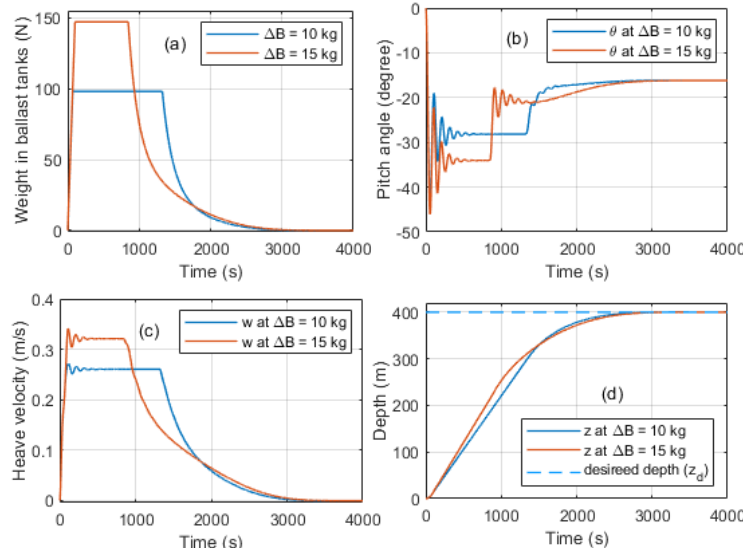


Figure 18. (a) Variation of the weight vs. time in ballast tanks, (b) pitch angle with time, (c) sinking (heave) velocity with time and (d) depth with time in closed loop for 5 m length AUV.

From these results we observe that the final achieved pitch angle is same as for the case of Design Example 1 (DE1). We note that for the DE2 the maximum sinking speed achieved is 0.35 m/s for 10 kg change in buoyancy and 0.44 m/s for 15 kg change in buoyancy. For the sake of clarification we can note here that the 10 kg change in buoyancy implies $\pm\Delta B$ of 20 kg and similarly 15 kg change in buoyancy implies $\pm\Delta B$ of 30 kg. Sinking speed becomes zero when the desired depth of hovering is achieved.

Figure 18a indicates variation of the weight with time in ballast tanks, Figure 18b indicates variation of the pitch angle with time, Figure 18c indicates variation of the sinking (positive heave) velocity with time and Figure 18d indicates variation of the depth with time in the closed loop condition for the 5 m length AUV. From these results we observe that the final achieved pitch angle is same as for the cases of DE1 and DE2. We note that for the DE3 the maximum sinking speed achieved is 0.26 m/s

for 10 kg change in buoyancy and 0.32 m/s for 15 kg change in buoyancy. As before, sinking speed becomes zero when the desired depth of hovering is achieved.

Critically through the discussions of DE1, DE2 and DE3, we note the following implementable guidelines:

- Because the final achieved pitch angle is same as for the cases of DE1, DE2 and DE3, it implies that the design model is performing properly.
- A higher $\pm\Delta B$ results in higher sinking speed, provided other parameters are kept constant.
- A higher length of the AUV results in lower sinking speed provided other parameters are kept constant.
- Proposed design approach is scalable and design alternatives can be generated for different set of requirements as placed by the owner or user agency.

6. Verification and Validation of the Results

In justification part of the present study we consider non-dimensionalized parameter and any non-dimensionalized parameter is known to remove the effects of size and other variations. We consider the two existing AUVs integrated with their buoyancy system and their comparative study is reported in terms of non-dimensionalized number. This number is γ and is defined as follows:

$$\gamma = \frac{\text{Net buoyancy change capacity}}{\text{Mass of the AUV}} \quad (37)$$

Finally, detailed comparison of the present approach with other existing models is reported in Table 8. Additionally, Figure 19 indicates the ratio of the buoyancy change to mass of the AUV versus terminal velocity for all the design examples of present paper and the same is compared with other existing research results.

Table 8. Comparative study between some existing model and proposed.

Parameters of Consideration	Tang [32]	Tangirala and Dzielski [4]	Present Approaches			
			L = 2.8 m	L = 4.0 m	L = 5.0 m	
Net buoyancy change of vehicle ($\pm\Delta B$) (kg)	0.05342	90.7	20	40	60	40
Terminal heave velocity (w) (m/s)	0.046	0.1524	0.4	0.35	0.44	0.26
Pitch angle (θ) (degree)	1.2	20.0	16.3	16.5	16.5	16.5
Mass of the vehicle (kg)	18	5000	308	888	888	1735
Ratio of buoyancy change to mass of AUV (γ)	0.003	0.018	0.065	0.045	0.068	0.023
						0.035

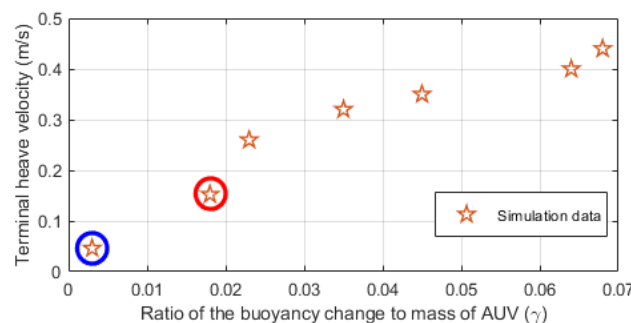


Figure 19. Ratio of the buoyancy change to mass of the AUV vs. terminal velocity (Note: Blue circle mark represents the result of Tang [32], Red circle mark represents the results of Tangirala and Dzielski [4], and all the others un-circled are our results).

From these results we note the following:

- Presented approaches offer the maximum ($\pm\Delta B/m$) and attains reasonably lower pitch angle which makes our approach highly useful for the practical design and application.

- As the γ increases, the terminal heave velocity also increases and our design approach offers the maximum terminal heave velocity in comparison to the existing research results. A high heave velocity is highly desired for defense related applications during attack, rescue and recovery operations of the AUVs.

- Our approaches are scalable while the others did not present a scalable approach and all of them restricted their design to a selected set of parameters. Additionally, in other works, the design was neither presented in reference to the AUV's design parameters nor the VBS design was presented in terms of mass flow rate, pump rpm and total desired change in buoyancy etc.

- Our results indicate a controlled and better emergency release and recovery due to high vertical speed and with reasonably low pitch angle.

With the above mentioned observation we can cautiously state that the presented approach is expected to be useful for the real applications in design and development of the VBS for AUVs for both civil and defense applications.

7. Conclusions

Herein, we presented the complete design and analysis of large capacity VBS for different requirements of change of buoyancy and the presented design approach is scalable. Detailed examples have been presented for the VBS of different buoyancy capacities in integration with their vehicle dynamics and the considered AUVs were of 2.8 m, 4 m and 5.0 m length with capabilities to operate/hover up to depth of 400 m. A CSM for all the three DEs has been presented to efficiently control the buoyancy and maximum sinking speed 0.44 m/s has been achieved with high value of ratio of buoyancy change to mass of AUV (γ). High sinking speed and γ are highly preferred in the design of VBS for both the civil and defense UVs. Results related to controller indicated robust and stable performances and the computed maximum pitch angles were 16.5 degrees for all the three DEs after reaching the desired depth of 400 m. Overall performance analyses indicate that using the state feedback LQR controller the AUVs will be able to hover at the desired depth with minimum amount of undesired oscillations and low power consumption.

Herein, we have not attempted any detailed energy efficiency analysis and in this study we have reported the simulation results only because the product realization is currently underway. Simulation results indicate the satisfactory performance of the vehicle during depth control and hovering operations at desired depth of operation. Experimental studies will be needed to confirm the performance of our proposed design. Herein, we have investigated the LQR controller and in future, other more advanced and robust controllers also can be investigated. For example: Digital Coefficient Diagram Method (DCDM), Proportional Derivative (PD), Proportional Integral Derivative (PID), fuzzy logic based controller, etc. These are currently under investigation and shall be reported later.

Author Contributions: Conceptualization, B.K.T. and R.S.; methodology, B.K.T. and R.S.; software, B.K.T.; validation, B.K.T. and R.S.; formal analysis, B.K.T.; investigation, R.S.; writing—original draft preparation, B.K.T.; writing—review and editing, R.S. and B.K.T.; visualization, B.K.T. and supervision, R.S. All authors have read and agreed to the published version of the manuscript.

Funding: This research was supported by the internal research grants of IIT Madras through research scheme: OE14D212 and from Marine Systems Panel, NRB, India via a sponsored project: NRB-263/MAR/12-13.

Acknowledgments: We thank the reviewers for their constructive comments which have helped immensely in improving the depth and clarity of paper. Also, we thank Awanish Chandra Dubey (Research Scholar, IIT Madras) for all of his technical discussions and help during this work.

Conflicts of Interest: The authors declare no conflict of interest.

Abbreviations

The following are the nomenclature and abbreviations used in this manuscript:

Nomenclature

β	Buoyancy capacity to weight ratio of the VBS	—
t	Thickness of the ballast tank	m
$\pm B$	Buoyancy capacity of the VBS	kg
N	Speed of the motor	rpm
m	Mass of the AUV	kg
U	Velocity of the AUV	m/s
V	Volume displaced by the AUV	m^3
V	Volume of the piston operated cylindrical ballast tank	m^3
η_{vol}	Volumetric efficiency of the ballast tank	—
η_a	Actuator efficiency	—
g	Gravitational acceleration	m/s^2
ρ	Density of the fluid	kg/m^3
L	Characteristic length of the AUV	m
D	Maximum diameter of AUV	m
L_n	Nose length of the AUV	m
L_m	Middle body length of the AUV	m
L_t	Tail length of the AUV	m
L_p	Length of the ballast tank of piston operated VBS	m
D_p	Diameter of ballast tank of piston operated VBS	m
A_{cs}	Cross sectional area of the piston operated VBS	m^2
C_d	Coefficient of drag	—
T_{rp}	Thrust required at piston head	$kg \cdot m/s^2$
γ	Ratio of buoyancy change to mass of AUV	—
K_c	Control gain matrix	—

Abbreviations

VBS	Variable Buoyancy System
BT	Ballast Tank
UV	Underwater Vehicles
EFF	Earth Fixed Frame
BFF	Body Fixed Frame
AUV	Autonomous Underwater Vehicles
AUG	Autonomous Underwater Gliders
BLDC	Brush-Less Direct Current
CoG	Center of Gravity
DOF	Degree Of Freedom
LQR	Linear Quadratic Regulator
MP	Motor for Pump
MFR	Mass Flow rate
RPM	Revolution Per Minute
CSM	Computer Simulation Model

Appendix A

Appendix A.1 Battery Selection

Parameters for the selection of battery: (1) Energy required for the mission and (2) energy density of the battery. Table A1a lists some of the existing options of batteries with their specific energy density and weight in kg for an energy capacity of 2.88 MJ.

Table A1. (a) List of options for different specific energy density and mass of battery for a specific energy capacity (E_R) adapted from Wang et al. [33] and Griffiths et al. [34] (b) Detailed specifications for different options of the PDP.

Battery	Types of Battery	Specific Energy Density (kJ/kg)	Weight in (kg)
Lithium Thionyl chloride	Primary	1512	$E_R/1512$
Lithium-ionCGR-18650HG	Secondary	576	$E_R/576$
Alkaline	Primary	396	$E_R/396$
Ni-metal hydride	Secondary	360	$E_R/360$
Lithium polymer	Secondary	342	$E_R/342$
Lead Acid Yuasa NPL78-12	Secondary	122.4	$E_R/122.4$

(b)			
Q (in cc/rev)	5.1	6.0	8.2
Operating speed (RPM)	1800	1800	1800
Mass flow rate (kg/min)	5.645	6.642	9.077
Maximum operating pressure (bar)	210	210	210
Weight of the PDP (kg)	2.7	2.8	2.90
Power required (watt)	369.23	434.39	593.66

Critical observations, guidelines and future scope: (1) Lithium thionyl chloride battery's specific energy density is very high in comparison to others, but it is not preferred because it of primary nature. (2) Secondary batteries can be recharged and because of this they are preferred. (3) Future seems to belong to the fuel cell. Nevertheless, at present there are issues related to their leakage (for more details see [35]) and because of this limitation at present this choice is restricted.

In this work, we select the option of Li-ion battery.

Appendix A.2 Pump Selection

Herein, our idea is to achieve the maximum change in buoyancy with minimum addition of weight and hence we analyze all the contributing weights. The weight of the pump depends on its mass flow rate capacity (Q in cc/rev) of the pump, design type, and operating pressure rating, etc.; in our analysis, we consider three PDP with varying capacities: 5.10, 6.0 and 8.20 cc/rev, adapted from [36].

Table A1b lists these detailed specifications and we note that the maximum operating pressure is 210 bar. In our design example the focus is on 400 m depth of operations and because of this the power required is computed only at 400 m depth for AUVs/AUGs which are integrated with our VBS. Hence power required by pump which is shown Table A1b is the power required at depth of 400 m for a particular flow rate capacity of pump. Available options for pumps are listed in Table A1b, and these are with the property of both directions of rotation, i.e., counter clock wise (CCW) and clock wise (CW) and their speeds range from 700 to 3000 RPM. Nevertheless, this study is based on the assumption that pumps is 60% efficient at 400 m operating depth and at 1800 RPM operating speed. The motor required to rotate the pump at a certain desired speed, will consume power differentially and a large required power will result into a high weight of the motor. For an efficient design, the flow rate of the pump is analyzed along with the power rating of motor and using these parameters we note that the weight of the motor for VBS is function of both depth of operation of VBS as well as mass flow rate.

Options for pump motor: Motor solutions to produce sufficient power at a depth of 400 m are: Option 1—using a BLDC motor GM80S-85B60 with weight of 1.7 kg, for 5.645, 6.64 kg/min and option 2—using the BLDC motor GM80S-105B60 with weight of 2.3 kg, for 9.077 kg/min, adapted from GEMS [37].

References

1. National Oceanic and Atmospheric Administration (NOAA). U.S. Department of Commerce, 2018. Available online: <https://oceanservice.noaa.gov/facts/exploration.html> (accessed on 19 February 2020).
2. Zhao, W.; Xu, J.A.; Zhang, M.J. A variable buoyancy system for long cruising range AUV. In Proceedings of the International Conference on Computer, Mechatronics, Control and Electronic Engineering (CMCE), Changchun, China, 24–26 August 2010.

3. Ferguson, J.S. The Theseus autonomous underwater vehicle. Two successful missions. In Proceedings of the IEEE International Symposium on Underwater Technology, Tokyo, Japan, 17 April 1998.
4. Tangirala, S.; Dzielski, J. A variable buoyancy control system for large AUV. *IEEE J. Ocean. Eng.* **2007**, *32*, 762–771. [[CrossRef](#)]
5. Aoki, T.; Tsukioka, S.; Yoshida, H.; Hyakudome, T.; Ishibashi, S.; Sawa, T.; Ohkusu, M. Advanced technologies for cruising AUV Urashima. *Int. J. Offshore Polar Eng.* **2008**, *18*, 81–90.
6. Hobson, B.W.; Bellingham, J.G.; Kieft, B.; McEwen, R.; Godin, M.; Zhang, Y. Tethys-class long range AUVs-extending the endurance of propeller-driven cruising AUVs from days to weeks. In Proceedings of the IEEE/OES autonomous underwater vehicles (AUV), Southampton, UK, 24–27 September 2012.
7. Brown, M.; Kelley, M.; McGill, P. MBARI vertical profiler. *MTS/IEEE Ocean.* **2001**, *4*, 2482–2485.
8. Sumantri, B.; Karsiti, M.N.; Agustiawan, H. Development of variable ballast mechanism for depth positioning of spherical URV. In Proceedings of the International Symposium on Information Technology, Kuala Lumpur, Malaysia, 26–28 August 2008; pp. 1–6.
9. Font, R.; Pelaez, J.G. On a submarine hovering system based on blowing and venting of ballast tanks. *Ocean Eng.* **2013**, *72*, 441–447. [[CrossRef](#)]
10. Woods, S.A.; Bauer, R.J.; Seto, M.L. Automated ballast tank control system for autonomous underwater vehicles. *IEEE J. Ocean. Eng.* **2012**, *37*, 727–739. [[CrossRef](#)]
11. Worall, M.; Jamieson, A.J.; Holford, A.; Neilson, R.D.; Player, M.; Bagley, P.M. A variable buoyancy system for deep ocean vehicles. In Proceedings of the OCEANS 2007–Europe, Aberdeen, UK, 18–21 June 2007; pp. 1–6.
12. Liu, Y.; Zhao, X.; Wu, D.; Li, D.; Li, X. Study on the control methods of a water hydraulic variable ballast system for submersible vehicles. *Ocean Eng.* **2015**, *108*, 648–661. [[CrossRef](#)]
13. Jensen, H.F. Variable Buoyancy System Metric. MS Thesis, Massachusetts Institute of Technology, Cambridge, MA, USA, 2009.
14. Riedel, J.S.; Healey, A.J.; Marco, D.B.; Beyazay, B. Design and Development of Low Cost Variable Buoyancy System for the Soft Grounding of Autonomous Underwater Vehicles. Available online: apps.dtic.mil/dtic/tr/fulltext/u2/a436027.pdf (accessed on 7 April 2020).
15. Webb, D.C.; Paul, J.S.; Jones, C.P. SLOCUM: An underwater glider propelled by environmental energy. *IEEE J. Ocean. Eng.* **2001**, *26*, 447–452. [[CrossRef](#)]
16. Curtin, T.B.; Bellingham, J.G.; Catipovic, J.; Webb, D. Autonomous oceanographic sampling networks. *Oceanography* **1993**, *6*, 86–94. [[CrossRef](#)]
17. Wood and Stephen. Autonomous underwater gliders, Published by IntechOpen. *Fla. Inst. Technol. USA* **2008**, *27*, 499–524.
18. Davis, R.E.; Erikson, C.C.; Jones, C.P. Autonomous buoyancy-driven underwater gliders. *Environ. Sci.* **2002**. [[CrossRef](#)]
19. Kojima, J.; Kato, Y.; Asakawa, K.; Matumoto, S.; Takagi, S.; Kato, N. Development of autonomous underwater vehicle 'AQUA EXPLORER 2' for inspection of underwater cables. *Conf. Proc. MTS/IEEE Ocean.* **1997**, *2*, 1007–1012.
20. Tiwari, B.K.; Sharma, R. A computing model for design of flexible buoyancy system for autonomous underwater vehicles and gliders. *Def. Sci. J.* **2018**, *68*, 589–596. [[CrossRef](#)]
21. Stock, A.; Kenneth, J.K. Comparing Performance and Efficiency of Linear Motors, Ball Screws, and Rack-and-Pinion Drives. Available online: www.machinedesign.com/archive/article/21829481/comparing-performance-and-efficiency-of-linear-motors-ball-screws-and-rackandpinion-drives (accessed on 19 February 2020).
22. Petersen, J.; Jacoby, R. Selecting positive displacement pumps: A wide variety of fluids are handled; understanding pump characteristics leads to the right choice. *Plant Eng.* **1993**, 138–140.
23. Raymond, R.J.; Young, W.C. *Roark's Formulae's for Stress and Strain*; McGraw-Hill: New York, NY, USA, 1989.
24. Fossen, T.I. *Handbook of Marine Craft Hydrodynamics and Motion Control*; John-wiley and Son's Ltd.: Hoboken, NJ, USA, 2011.
25. Prestero, T. Verification of a Six-Degree of Freedom Simulation Model for the REMUS Autonomous Underwater Vehicle. MS Thesis, Massachusetts Institute of Technology, Cambridge, MA, USA.
26. Graver, J.G. Underwater Gliders: Dynamics, Control and Design. Ph. D Thesis, Princeton University, Princeton, NJ, USA.

27. Leo, V.S.; Alexander, B.P.; Eric, R.; Maaten, E.F.; Stephen, R.T. Control of an AUV from Thruster Actuated Hover to Control Surface Actuated Flight. Available online: www.researchgate.net/publication/270587463_Control_of_an_AUV_from_thruster_actuated_hover_to_control_surface_actuated_flight (accessed on 7 April 2020).
28. Stephen, B.; Craig, B. *Linear Controller Design-Limits of Performance*; Prentice-Hall: Upper Saddle River, NJ, USA, 1991.
29. Katsuhiko, O. *Modern Control Engineering*, 9th ed.; Prentice-Hall: Upper Saddle River, NJ, USA, 2010.
30. Beyazay, B. Simulation and Modeling of a Soft Grounding System for an AUV. MS Thesis, Naval Postgraduate School, Monterey, CA, USA.
31. Tiwari, B.K.; Sharma, R. Design and development of a pump-driven variable buoyancy engine for autonomous underwater vehicles/gliders. In *Advances in Simulation, Product Design and Development, Multidisciplinary Industrial Engineering*; Springer: Singapore, 2020.
32. Tang, S.C. Modeling and Simulation of the Autonomous Underwater Vehicle Autolycus. MS Thesis, Massachusetts Institute of Technology, Cambridge, MA, USA, 1999.
33. Wang, W.H.; Engelaar, R.C.; Chen, X.Q.; Chase, J.G. The State-of-Art of Underwater Vehicles Theories and Applications. Available online: www.researchgate.net/publication/45237262_The_State-of-Art_of_Underwater_Vehicles_-_Theories_and_Applications (accessed on 7 April 2020).
34. Griffiths, G.; Jamieson, J.; Mitchell, S.; Rutherford, K. Energy storage for long endurance AUVs. Autonomous Undersea Vehicle Applications Center Publication, 8–16. Available online: auvac.org/uploads/publication_pdf/Energy%20Sys%20for%20long%20Endure%20AUV.pdf (accessed on 7 April 2020).
35. Jiaqing, H. Safety Study Related to Hydrogen Leakage from Fuel Cell Systems. MS Thesis, Concordia University, Montreal, QC, Canada, 2017.
36. Eaton External Gear Pump: GD5—Series E-PUGE-CC001-E, December 2014. Available online: www.eaton.in/ecm/groups/public/@pub/@eaton/@hyd/documents/content/pct_1200103.pdf (accessed on 19 February 2020).
37. Global Electric Motor Solutions, Manufacturer/Supplier of Small Electric Motors for a Variety Engineering and Industry Applications. Available online: gemsmotor.com/bldc/nema32-brushless-dc-motor.pdf (accessed on 19 February 2020).



© 2020 by the authors. Licensee MDPI, Basel, Switzerland. This article is an open access article distributed under the terms and conditions of the Creative Commons Attribution (CC BY) license (<http://creativecommons.org/licenses/by/4.0/>).